이학석사 학위논문

Star Formation Activity of Galaxies Undergoing Ram Pressure Stripping in the Virgo Cluster

처녀자리 은하단에서 충차압에 의한 가스 손실을 겪는 은하들의 항성 형성 활동

2020년 8월

서울대학교 대학원

물리·천문학부 천문학전공

문 재 연

Star Formation Activity of Galaxies Undergoing Ram Pressure Stripping in the Virgo Cluster

처녀자리 은하단에서 충차압에 의한 가스 손실을 겪는 은하들의 항성 형성 활동

지도교수 이 명 균

이 논문을 이학석사 학위논문으로 제출함

2020년 4월

서울대학교 대학원

물리·천문학부 천문학전공

문 재 연

문 재 연의 이학석사 학위논문을 인준함

2020년 6월

위 원 장 구 본 철

부 위 원 장 이 명 균

위 원 임 명 신

ABSTRACT

We study galaxies undergoing ram pressure stripping in the Virgo cluster to examine whether we can identify any discernible trend in their star formation activity. We first use 48 galaxies undergoing different stages of stripping based on HI morphology, HI deficiency, and relative extent to the stellar disk, from the VIVA survey (VLA Imaging survey of Virgo galaxies in Atomic gas). We then employ a new scheme for galaxy classification which combines HI mass fractions and locations in projected phase space, resulting in a new sample total of 241 galaxies. We utilize a variety of star formation tracers, which include $g - r$, *WISE* [3.4] − [12] colors, and starburstiness that are defined by stellar mass and star formation rates to compare the star formation activity of galaxies at different stripping stages. We find no clear evidence for enhancement in the integrated star formation activity of galaxies undergoing early to active stripping. We are instead able to capture the overall quenching of star formation activity with increasing degree of ram pressure stripping, in agreement with previous studies. Our results suggest that if there is any ram pressure stripping induced enhancement, it is at best locally modest, and galaxies undergoing enhancement make up a small fraction of the total sample. Our results also show that it is possible to trace galaxies at different stages of stripping with the combination of HI gas content and location in projected phase space, which can be extended to other galaxy clusters that lack high-resolution HI imaging.

Keywords: galaxies: clusters: general − galaxies: clusters: individual (Virgo) − galaxies: evolution − galaxies: star formation

Student Number: 2018-26181

Contents

List of Figures

List of Tables

Chapter 1

Introduction

[1] Star formation and nuclear activity of galaxies are strongly affected by the cluster environment (von der Linden et al. 2010; Hwang et al. 2012a) through various physical mechanisms: ram pressure stripping (Gunn & Gott 1972), thermal evaporation (Cowie & Songaila 1977), strangulation (Larson et al. 1980; Bekki et al. 2002), galaxy harassment (Moore et al. 1996), and cumulative galaxy-galaxy hydrodynamic/gravitational interactions (Park & Hwang 2009). Among them, ram pressure stripping is one of the most effective ways to remove gas from galaxies. Ram pressure arises due to the hot X-ray gas embedded in the intracluster medium (ICM), and pushes against the interstellar medium (ISM) of a galaxy as the galaxy travels through the cluster. As a galaxy approaches the cluster core, the strength of ram pressure increases, and a greater amount of its gas - the fuel necessary for star formation - is stripped (Gunn & Gott 1972). In general, ram pressure stripping (RPS) is expected to quench star formation in cluster galaxies (e.g., Koopmann & Kenney 2004b; Crowl & Kenney 2008; Jaffé et al. 2015). However, there have been observational and theoretical studies insinuating the possi-

[1]The content of this thesis has been submitted to the Journal of the Korean Astronomical Society for review.

bility of ram pressure induced star formation enhancement prior to quenching (e.g., Bothun & Dressler 1986; Fujita & Nagashima 1999; Kronberger et al. 2008; Kapferer et al. 2009). One-sided tails of Hα emission or young stellar knots extending beyond disks of galaxies in distant clusters have shown to be linked to interactions with the ICM (e.g., Cortese et al. 2007; Hester et al. 2010; Smith et al. 2010), giving further support to the scenario of ram pressure induced star formation enhancement. While not all galaxies subject to ram pressure stripping show such features, those that exhibit extended tails of optically bright gas are known as "jellyfish" galaxies. As of recent, many observational studies of jellyfish galaxies have captured the enhancement of star formation activity in their disks and tails (Vulcani et al. 2018; Ramatsoku et al. 2019). In particular, Vulcani et al. (2018) categorized their sample of jellyfish galaxies from the GAs Stripping Phenomena survey (GASP; Poggianti et al. 2017) into different stripping stages - initial, moderate, and extreme stripping, along with truncated disks - based on their Hα morphology. Upon comparing the star formation activity of their sample to field galaxies of similar stellar mass, they show that jellyfish galaxies undergoing moderate to extreme stripping show the strongest enhancement of star formation. As such, it is of great interest to probe the change in star formation activity of a galaxy as it undergoes different stages of ram pressure stripping.

Given its close proximity, the Virgo cluster has often been the target of observational studies of interstellar medium (ISM) - intracluster medium (ICM) interactions. Koopmann & Kenney (2004b) studied the Hα morphology of Virgo cluster and isolated spiral galaxies to not only divide cluster galaxies into different categories - normal, anemic, enhanced, and truncated - but also to identify the history of environmental processes that galaxies may have experienced in the cluster environment. While Hα is a useful probe of the current star formation activity, the distribution of neutral hydrogen (HI) of a galaxy offers a clearer picture of the environmental processes a galaxy has undergone.

Given that HI gas is usually extended out towards the outer disk region of a galaxy, it is often the first component to show perturbations due to external processes such as tidal interactions and ram pressure stripping. Chung et al. (2009) obtained high-resolution HI data of a sample of 53 late type galaxies in the Virgo cluster, among which 46 of them were selected based on the classification in Koopmann & Kenney (2004b) to probe galaxies with a wide range of star formation properties. Known as the VLA Imaging survey of Virgo galaxies in Atomic gas (VIVA), Chung et al. (2009) identified a trend in HI morphology with respect to the projected location of galaxies within the cluster. Galaxies near or in the core were often found with symmetric HI disks truncated with respect to their stellar disks, while galaxies in the outskirts were generally HI-rich in comparison. On the other hand, galaxies located at intermediate distances from the cluster core (i.e., M87; $0.6 \lesssim d_{M87} \lesssim 1$ Mpc) were observed to have one-sided HI tails pointing away from the core, which led Chung et al. (2007) to suggest that such galaxies have only recently began falling into the cluster, and that the impact of ram pressure on the gas content of galaxies extends out towards intermediate distances.

It is then possible to infer from the results of previous studies that the combination of HI morphology and projected location from the cluster center can offer a closer look into the orbital history of a galaxy within a galaxy cluster. As of recent, many studies have incorporated the use of projected clustercentric distance and line-of-sight velocity with respect to the cluster mean in the form of a phase-space diagram to identify galaxies at different stages in their orbits (Oman et al. 2013; Oman & Hudson 2016; Rhee et al. 2017). For example, Jaffé et al. (2015) studied Abell 963, a galaxy cluster at z = 0.2, by combining the availability of HI detections and location in projected phase space. They found that HI-detected galaxies were generally located in the "recent infalls" region, whereas there was a noticeable lack of HI-detections within the "stripped" and "virialized" regions. Moreover, they investigated the stellar populations of their galaxy

sample using $NUV - r$ color to find that the bluest galaxies were generally found outside the "stripped" and "virialized" zones, while the redder galaxies seemed to dominate those two regions. While they were not able to take HI morphology into account for their analysis, their results confirm the general trend that as blue, star-forming galaxies fall into a cluster, its gas content will be gradually stripped by ram pressure as it settles, with its star formation being quenched in the process.

Given that observational studies of jellyfish galaxies have shown that a stage of star formation enhancement could occur prior to its gas content being completely quenched, this then brings up the question of whether a similar analysis can be done for the Virgo cluster. Yoon et al. (2017) provides an ideal sample to answer such a question, as they have used the VIVA (Chung et al. 2009) sample to categorize galaxies in the Virgo cluster into different stages of stripping based on their HI morphology, HI deficiency ($\mathrm{def_{HI}}$, a measure of how deficient in HI a galaxy is relative to its field counterpart of the same size, Haynes & Giovanelli 1984), and relative extent to the optical disk. The availability of high-resolution HI imaging plays a crucial role in their study, as the peculiarities in the HI morphology allows a direct probe of the environmental processes that the galaxy may have been subject to. Yoon et al. (2017) also briefly examined the star formation properties of the categorized galaxies using the Hα equivalent width and Hα concentration from Koopmann & Kenney (2004a). Their results (see Yoon et al. 2017, Fig. 8) showed reduced star formation and increased concentration of star formation in the galaxy center, along with decreasing HI gas content from early through post stripping stages.

In this work, we aim to build upon the work of Yoon et al. (2017) by examining the star formation properties of their sample of galaxies in more detail, using various types of star formation tracers. To make up for the small sample size in their study, we expand the sample by using the Extended Virgo Cluster Catalog (EVCC; Kim et al.

2014). Since high-resolution HI data are not available for the entirety of the EVCC, we make use of HI mass fraction (relative HI mass to stellar mass, M_{HI}/M_*) and location in projected phase space. While M_{HI}/M_* can work as a first-order indicator of gas stripping, the location of galaxies in phase space assures that the origin of stripping is likely to be of ram pressure (Rhee et al. 2017; Jaffé et al. 2015; Yoon et al. 2017).

This paper is organized as follows. In Section 2, we describe the sample and explain the derivation of physical properties used to examine the star formation activity of galaxies in the Virgo cluster. In Section 3, we explain how the different stripping classes were defined in both Yoon et al. (2017) and this study, following up with the analysis of the star formation activity per class. In Section 4, we discuss the limitations of integrated properties in capturing local star formation enhancements in Virgo galaxies, and how the simplification of the classification scheme using HI gas fraction and location in phase space allowed the trend of quenching of star formation activity to be observed with a larger sample. We summarize our results in Section 5. Throughout this paper, we adopt a Salpeter (Salpeter 1955) initial mass function (IMF) and assume a Λ cold dark matter cosmology with $\Omega_M = 0.3$, $\Omega_\Lambda = 0.7$, and $H_0 = 70$ km s^{-1} Mpc^{-1}. We also adopt a distance of 16.5 Mpc, or $(m-M) = 31.1$, to the Virgo cluster (Mei et al. 2007). All photometric magnitudes used are given in the AB magnitude system.

Chapter 2

Data

2.1 EVCC

The EVCC is comprised of fundamental information such as cluster membership, morphology, radial velocities, and *ugriz* photometry of a total of 1589 galaxies spread throughout the main body to the outskirts of the Virgo cluster. More precisely, the spatial coverage of the EVCC extends out to ∼4 times the virial radius (r_{200} = 1.55 Mpc, McLaughlin 1999; Ferrarese et al. 2012) of the cluster, for which Kim et al. (2014) excluded background galaxies with radial velocities larger than 3000 km s^{-1}.

With regards to the *ugriz* photometry, the Sloan Digital Sky Survey (SDSS) photometric pipeline is known to be unreliable for large and bright galaxies due to issues with deblending and sky subtraction (Abazajian et al. 2004, 2009; West et al. 2010). To account for such shortcomings, Kim et al. (2014) performed their own Source Extractor (SExtractor, Bertin & Arnouts 1996) photometry on *ugriz* images from SDSS Data Release 7 (DR7). As shown by Figure 13 in Kim et al. (2014), the growing discrepancy between the photometric magnitudes with increasing angular size of a galaxy further confirms that the total flux derived from the SDSS pipeline does not give an accurate

representation of the total light from nearby galaxies such as those in the Virgo cluster. We thus attest that physical parameters derived using EVCC *ugriz* photometry, such as stellar mass, are reliable measurements of the stellar population of the galaxies in the Virgo cluster.

2.2 Physical Parameters of Galaxies

To examine the star formation properties of Virgo cluster galaxies, we proceed by building a master catalog based on the EVCC. We add stellar masses, star formation rates (SFRs), mid-infrared photometric data, along with neutral hydrogen masses to the catalog. Here, we briefly describe each of the physical parameters.

2.2.1 Stellar Masses

The stellar masses of EVCC galaxies are computed using *Le Phare* (Arnouts et al. 1999; Ilbert et al. 2006). We used EVCC *ugriz* photometry and redshifts to build synthetic spectral energy distributions (SEDs) from the stellar population synthesis (SPS) models of Bruzual & Charlot (BC03; 2003), which are based on the Chabrier (2003) IMF. The synthetic SEDs are computed at different redshifts with $\delta z = 0.001$ as the furthest galaxy in our sample is located at z $\sim$ 0.01. The BC03 templates provided by *Le Phare* have three metallicities and seven exponentially decreasing star formation models (SFR $\propto e^{-t/\tau}$) with τ = 0.1, 0.3, 1, 2, 3, 5, 10, 15, and 30 Gyr. We allow the age of the stellar population to vary between 0 and 13 Gyr. Dust extinction was applied to the SPS templates using the extinction law of Calzetti et al. (2000), with values of $E(B-V)$ varying from 0 to 0.6. Adopting different values of the stellar population parameters gives rise to a distribution of different estimates for the stellar mass of each galaxy. We adopt the median of the distribution as the stellar mass of each galaxy.

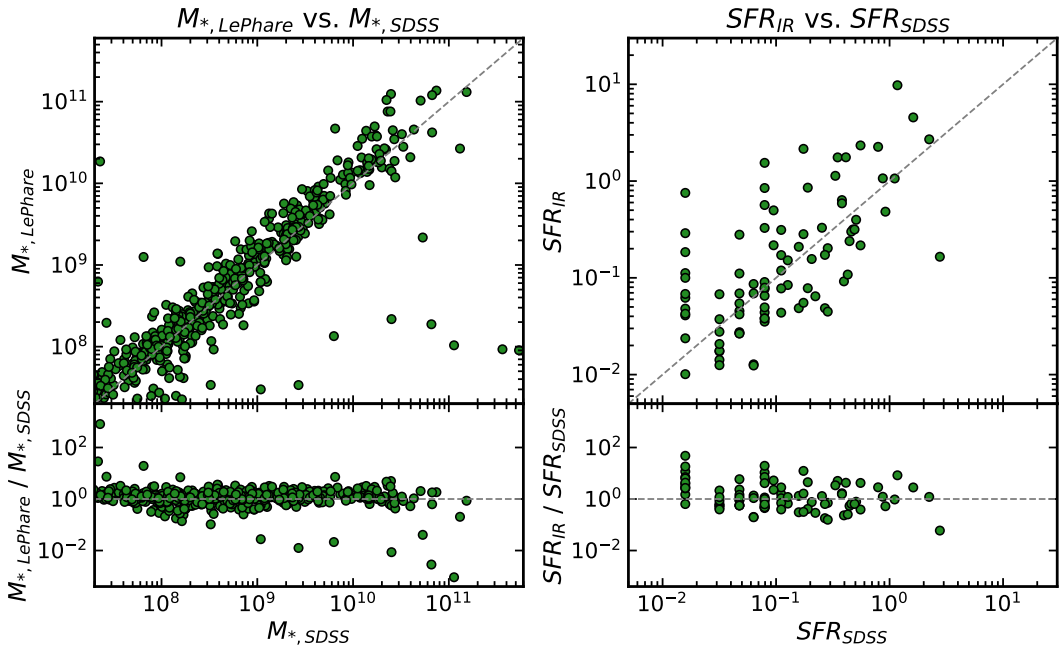

Figure 2.1. Comparison diagram of stellar masses measured via an SED fit of EVCC *ugriz* photometry with *Le Phare* (left), and star formation rates derived using total IR luminosities with those given in the SDSS MPA/JHU DR7 VAGC. The dashed lines in the top panels show the one-to-one relations.

We compare our stellar mass estimates with those given by the SDSS MPA/JHU DR7 VAGC (Kauffmann et al. 2003), where stellar masses were measured based on a SED fit of SDSS *ugriz* photometry with the SPS models of Bruzual & Charlot (2003). The stellar mass estimates from the MPA/JHU DR7 VAGC are based on the Kroupa IMF. For consistency throughout this study, stellar mass estimates computed via *Le Phare* and those given by the MPA/JHU DR7 VAGC are converted to a Salpeter (1955) IMF by multiplying the former by a factor of $10^{0.25}$ (Chabrier 2003) and the latter by a factor of $10^{0.2}$ (Kroupa 2001). Both conversion factors were taken from Bernardi et al. (2010). We show the results of the comparison in the left panel of Figure 2.1, which shows good agreement between the two stellar mass estimates with a median offset of about 0.08 dex. While there is in general a good agreement between the two methods, the rms of the difference between our estimates and those given by the MPA/JHU DR7 VAGC is about 0.49 dex when including all the galaxies in common. The absolute uncertainty arising from panchromatic SEDs is approximately 0.3 dex (Conroy 2013). The large rms can be attributed to the outliers, for which some of them can be explained by the large magnitude offset between EVCC and SDSS photometry. As mentioned in Section 2.1, there have been known issues with the SDSS photometric pipeline with regards to bright, nearby galaxies. Excluding the outliers with 2-sigma clipping from the sample results in a rms of $\sim$0.23 dex, which suggests that our stellar mass estimates are overall consistent with the measurements given by the SDSS MPA/JHU DR7 VAGC.

2.2.2 Star Formation Rates & Mid-Infrared Colors

We use mid-infrared photometric data from the *Wide-field Infrared Survey Explorer* (*WISE*, Wright et al. 2010) to derive SFRs and examine mid-infrared colors. The *WISE* survey covers the entire sky in the mid-infrared, offering four-band photometric data (3.4, 4.6, 12, and 22μm) for over 747 million objects. We used a matching tolerance of

$6''$ ($\sim$FWHM of the PSF at 3.4μm) between the EVCC and AllWISE Source Catalog[1]. In the cross-matching process, we found some issues with the coordinates given by the EVCC. EVCC provides two different coordinates, one derived from SExtractor, another given by the SDSS fiber locations. The coordinates given by SExtractor were offset from the center of nearby galaxies, resulting in an offset as large as $\sim$13.68$''$ in one particular case. Given that the galaxies with the largest offsets were those with high-resolution HI imaging used in Yoon et al. (2017), it was necessary to ensure that these galaxies could be found within a matching tolerance of $6''$. We thus replaced the coordinates of Yoon et al.'s 48 galaxies with those given by the NASA Extragalactic Database (NED). For 2 galaxies with no match, the NED-given coordinates are replaced with *WISE*-given coordinates of the closest *WISE* detection in the AllWISE Source Catalog. There were 4 additional galaxies in the EVCC that were not found within the matching tolerance, which were manually searched for and added to the master catalog. The AllWISE Source Catalog provides both point source profile-fitting and elliptical aperture magnitudes. Because we are dealing with nearby galaxies, some of them are well-resolved to the point that we generally require larger apertures to obtain an accurate measurement of their total brightness. We thus prioritize the use of elliptical aperture magnitudes for galaxies in the EVCC. For those with no elliptical magnitudes given by the AllWISE Source Catalog (i.e., relatively small galaxies), we use point source profile-fitting magnitudes instead. We also select reliable flux density values with a signal-to-noise ratio cut of S/N $\geq$ 3 in each band.

To compute SFRs, we use *WISE* 22μm flux densities, which were shown to be reliable SFR indicators in Hwang et al. (2012c) and Lee et al. (2013). We derive total infrared (IR) luminosities from *WISE* 22μm luminosities using the SED templates of Chary & Elbaz (2001). We then convert the total IR luminosities into SFRs with the

[1] `http://wise2.ipac.caltech.edu/docs/release/allwise/`

Kennicutt (1998) relation, assuming a Salpeter IMF: SFR_{IR} ($M_\odot$ yr^{-1}) = 1.72 × 10^{-10} L_{IR} ($L_\odot$). We remove active galactic nuclei (AGN) from the sample to avoid contamination in the mid-infrared. We identify 21 AGN via the Baldwin-Phillips-Terlevich (BPT) classification provided by the MPA/JHU DR7 VAGC. We also use the *WISE* mid-infrared color-color selection criteria defined by Jarrett et al. (2011) and Mateos et al. (2012) to identify one additional AGN. A total of 24 AGN, including 2 composite galaxies with large offsets from the one-to-one relation in Figure 2.1 (via 2-sigma clipping), were identified and removed from the sample.

We then compare our SFR estimates with those in the MPA/JHU DR7 VAGC (Brinchmann et al. 2004) in the right panel of Figure 2.1. The SFRs in the MPA/JHU DR7 VAGC were derived from extinction and aperture-corrected Hα luminosities. For AGN and galaxies with weak emission lines, they measure the SFRs using the 4000 Å (D_n4000) break. There seems to be a correlation between the two measurements despite a large scatter. The median offset between SFR_{IR} and SFR_{SDSS} is approximately 0.03 dex. The data with the largest offsets can be explained by a number of factors. Upon comparison of SDSS and *WISE* images, we find 3 star-forming galaxies with relatively large measurements of SFRs in the infrared (offset on the order of $\gtrsim$1 dex) to be barred spiral galaxies. We attribute the likely cause of this discrepancy to the fact that SDSS fiber observations were limited to the central part of the galaxies with low star formation activity, thus leading to an underestimation of the SFR despite aperture corrections. We also examine star-forming galaxies with large offsets on the other end, i.e., those with larger measurements of the star formation rate in Hα. Two of them are identified as irregular galaxies, which makes sense as UV bright galaxies that consist entirely of young stellar populations (and thus do not contain much dust) would result in a very weak detection in *WISE* 22μm. This would in turn result in a higher measurement of the SFR in Hα and a lower measurement of the SFR in the infrared.

2.2.3 Atomic Gas Masses

We adopt the atomic gas masses, M_{HI}, from the Arecibo Legacy Fast ALFA Survey (ALFALFA, Giovanelli et al. 2005; Haynes et al. 2011, 2018). The latest release, the ALFALFA Extragalactic HI Source catalog (Haynes et al. 2018), provides HI data for a total of ∼31,500 extragalactic sources detected out to $z < 0.06$. We cross-match the catalog with the EVCC within a matching tolerance of $4''$, giving a total of 579 matched objects. Among the 579 matched objects, there are a total of 39 galaxies with RPS classes defined by Yoon et al. (2017). The HI detection limit for the ALFALFA survey is about 10^6 $M_\odot$, and the stellar mass of our sample ranges from about 2×10^7 $M_\odot$ to 6×10^{11} $M_\odot$. This indicates that the lowest valid value of the relative HI-to-stellar mass ratio for our sample is approximately 2×10^{-6}, which is equivalent to a logarithmic value of -5.8. Our lowest measured value gives a logarithmic value of -2.97, suggesting that all our measurements of the HI mass fractions are valid.

Chapter 3

Results

3.1 Star Formation Properties of Galaxies Undergoing Different Stages of RPS

3.1.1 Definition of RPS Classes

Yoon et al. (2017) categorize a total of 35 galaxies into different stages of stripping and identify an additional class of 13 control galaxies that are not subject to stripping. Characterization of each class is briefly described in Table 3.1, adapted from Table 1 and Section 2 in Yoon et al. 2017. Among the stripping classes, Classes I, II, and III represent galaxies undergoing early, active, and post stripping stages, respectively. On the other hand, galaxies that show no strong evidence of stripping due to the ICM are utilized as a control sample, labeled as Class 0 (N = 13), whereas galaxies that appear to have lost HI gas at all radii due to a mechanism other than ram pressure stripping, such as starvation (Larson et al. 1980), are labeled as Class IV (N = 8).

Table 3.1. The VIVA sample defined by different stages of gas stripping

Class	def_{HI} (Range)	def_{HI} (Median)	HI morphology and deficiency compared to field galaxies
(1)	(2)	(3)	(4)
Class 0 (N = 13)	-0.81 $\sim$ 0.38	0.13	No definite signs of gas stripping due to the ICM
Class I (N = 7)	-0.43 $\sim$ 0.41	0.02	One-sided HI feature; relatively comparable to field galaxies in HI gas content
Class II (N = 10)	0.12 $\sim$ 1.16	0.76	Highly asymmetric HI disk; quite deficient in HI, with an average of $\sim$17% of HI mass compared to those of field galaxies.
Class III (N = 10)	0.82 $\sim$ 2.25	1.42	Symmetric and severely truncated HI disk; extremely deficient in HI, with $<$4% of the HI mass of a field counterpart.

Class IV (N = 8)	0.51 $\sim$ 1.17	0.79	Symmetric HI disk with marginal truncation within the radius of the stellar disk; lower HI surface density than other classes; quite deficient in HI with on average $\sim$15% of the HI mass of a field counterpart.

(1) RPS class, (2) HI deficiency range, (3) median HI deficiency, (4) HI morphology and relative HI deficiency compared to those of field galaxies. Table adapted from Yoon et al. (2017).

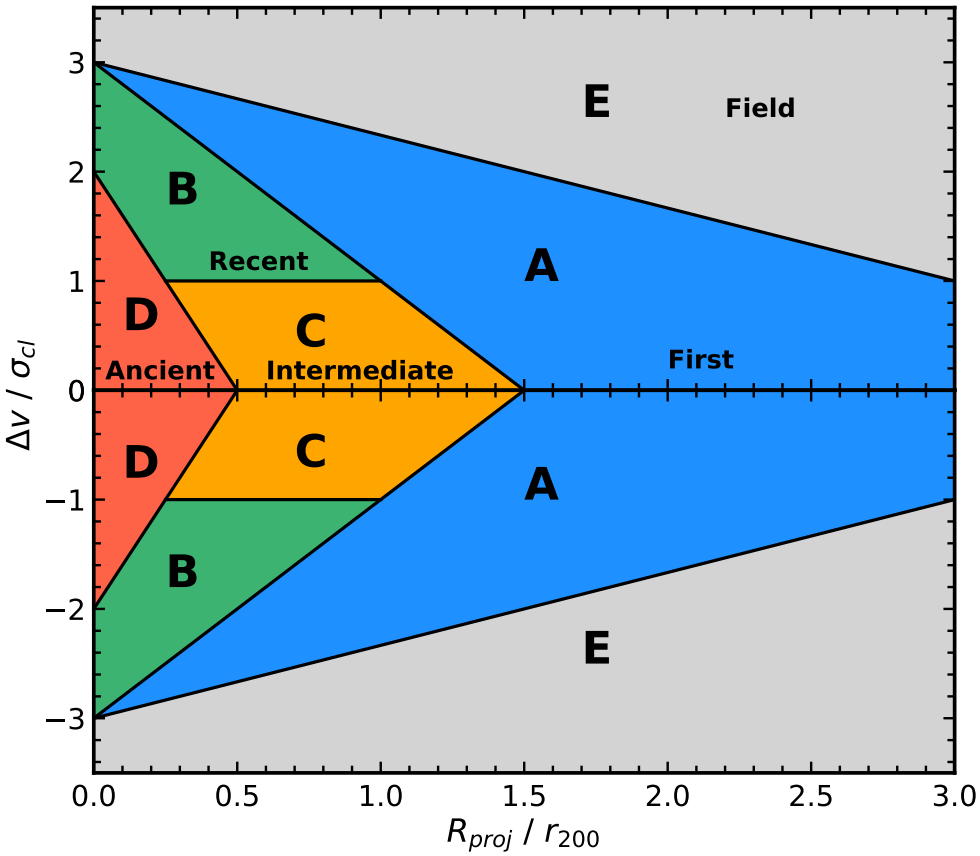

Figure 3.1. Projected phase-space diagram with regions A ∼ E defined according to time since infall into the cluster center, closely following the classification in Rhee et al. (2017). Clustercentric distance and velocity are normalized by the cluster virial radius r_{200} and cluster velocity dispersion σ_{cl}, respectively. First infallers are located in Region A, recent infallers in Region B, intermediate infallers in Region C, and ancient infallers in Region D. Region E is defined by field galaxies.

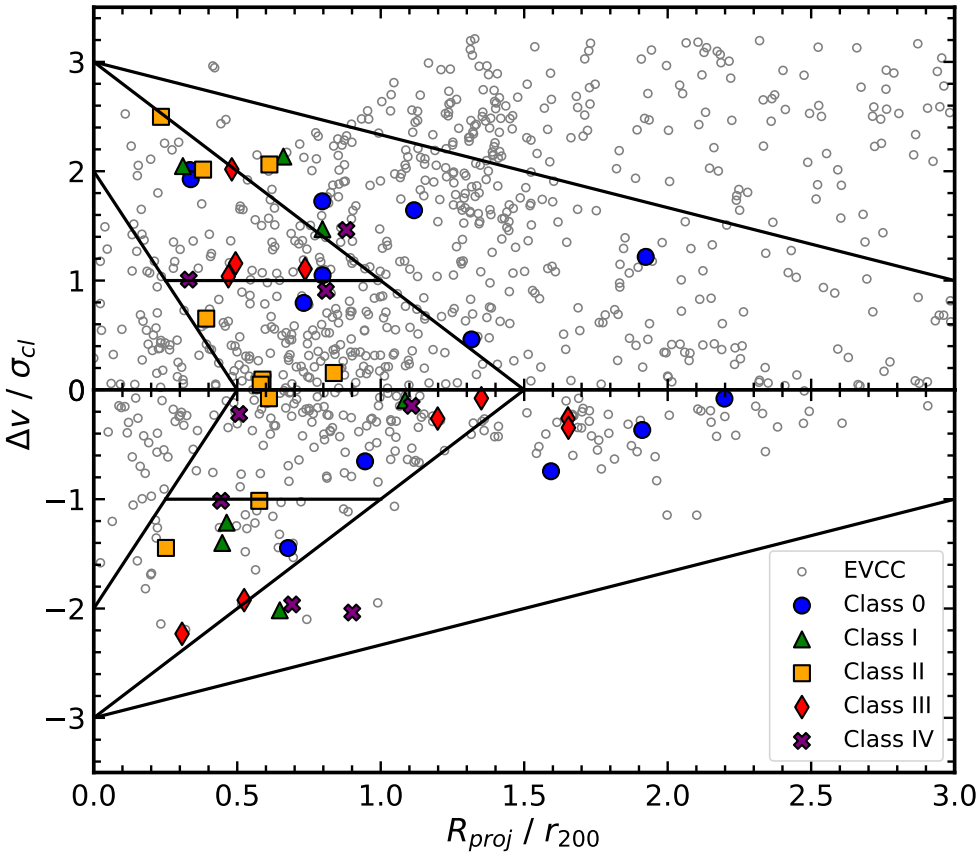

Figure 3.2. Projected phase-space diagram of RPS class galaxies and the rest of the EVCC sample shown as reference (grey open symbols).

Yoon et al. utilize these five classes in combination with projected phase space to better trace the orbital histories of HI stripped galaxies within the Virgo cluster. Given the large scatter in projected phase space due to projection effects (e.g., Oman et al. 2013; Rhee et al. 2017), the availability of high-resolution HI imaging plays an important role in identifying the orbital stage of the selected galaxies. We plot the locations of RPS class galaxies, along with other EVCC galaxies, in projected phase space in Figure 3.2. In the diagram, we can clearly see that our reference sample is not uniformly distributed in projected phase space, such that they preferentially inhabit regions with positive clustercentric velocities. We attribute the cause of this non-uniformity to the limited sky coverage of the EVCC. Yoon et al. find reference galaxies traveling at positive velocities to be consistent with the NGC 5353/4 filament and the W-M sheet (Kim et al. 2016), which are found to be located behind the Virgo cluster. On the other hand, Kim et al. (2016) also find filamentary structures located in front of and/or in the vicinity of Virgo, to be elongated towards the cluster, indicating cluster infall. However, these structures fall outside of the sky coverage of the EVCC, which explains the absence of galaxies in the bottom half of the phase-space diagram.

In Figure 3.1, we label different regions in projected phase space according to time since infall, using a modification of the classification adopted by Rhee et al. (2017). According to the expected orbit of a radially infalling galaxy (e.g., Yoon et al. 2017; Rhee et al. 2017; Jaffé et al. 2015), a galaxy under the influence of the cluster potential will slowly accelerate from the outskirts to eventually virialize in the cluster core after multiple core crossings. Classes I $\sim$ III overall follow the expected trend of radially infalling galaxies within projected phase space, as shown in Figure 3.2. Class I galaxies are located at high velocity and low to intermediate clustercentric distances, which in combination with their HI morphology, show that they are likely to be on their first infall into the cluster core. Class II galaxies are at similar locations in projected

phase space as Class I galaxies, with a select few found to be traveling at relatively low velocities. For the latter, Yoon et al. suggest that tidal interactions may cause a shift in projected phase space, and thus caution is advised when interpreting their locations with respect to their orbital histories. Although some Class III galaxies are found in the same region in projected phase space as Class II/I objects, their heavily truncated HI disks suggest that they have already experienced their first core crossing, and are now falling out of the core. HI morphology alone suggests that Class III galaxies are at a later stripping stage than Class II galaxies are. However, their relative locations in projected phase space imply that a subsample of Class II galaxies are at a later stage in their orbital histories relative to some Class III galaxies. Yoon et al. therefore suggest that Class III galaxies do not always occur after Class II. Among the Class III galaxies, there are a subsample of them found at radii beyond the cluster virial radius (i.e., $R_{proj}/r_{200} = 1$), for which Yoon et al. identify as a backsplashing population. While Class IV galaxies are generally found at low to intermediate clustercentric distances, they are rather spread out in projected phase space. Class 0 galaxies also exhibit a large scatter in projected phase space, although more than half of them are found in the first infalls (i.e., Region A) region. With the exception of galaxies subject to other stripping mechanisms such as tidal interactions and starvation, or those that do not seem to show any signs of gas depletion, Yoon et al. demonstrate that the combination of HI morphology and location in projected phase space enriches the information one can obtain with regards to the orbital history of galaxies within a galaxy cluster.

3.1.2 Star Formation Properties of Galaxies with Different RPS Classes

We examine the star formation properties of galaxies undergoing different stages of ram pressure stripping, using star formation tracers sensitive to a broad range of star-forming timescales. We use $\mathrm{SFR_{IR}}$, $g - r$, and *WISE* [3.4] − [12] colors. We plot these

star formation tracers against stellar mass in Figure 3.3. For SFR_{IR}, we adopt the main sequence defined in Elbaz et al. (2007), which was derived from a best linear fit of star-forming SDSS galaxies at $0.015 \leq z \leq 0.1$. The solid line represents the main sequence, with the dashed lines representing the lower and upper bounds to the main sequence fit. The optical color $g - r$ can also work as a tracer of star formation activity (Strateva et al. 2001; Blanton et al. 2003). We define a red sequence using the best linear fit of non-RPS class galaxies with $M_* > 1.5{\times}10^{10}$ $M_\odot$ and $g - r > 0.58$. The mid-infrared $[3.4] - [12]$ color is a tracer of recent star formation activity in a galaxy, up to $\sim$2 Gyr timescales (e.g., Ko et al. 2013). We adopt the peak of the mid-infrared color distribution of star-forming galaxies (i.e., $[3.4] - [12] = 1$) from Hwang et al. (2012b) as the star-forming sequence.

Largely due to small number statistics of the RPS class sample, it is difficult to identify a trend in the star formation activity of RPS class galaxies from Figure 3.3 alone. Overall, galaxies in the Virgo cluster appear to have lower current star formation rates relative to the star-forming main sequence. There are a select few Class 0 and I galaxies found above the main sequence. However, there are also some others that appear to be less star-forming compared to other RPS class galaxies that are far more deficient in HI. We note that the main sequence adopted here was based on a best linear fit of galaxies located at $0.015 \leq z \leq 0.1$ (see Elbaz et al. 2007, Figure 18), and thus may not be an accurate representation of the main sequence for galaxies at $z \lesssim 0.01$, which is the case for galaxies in the EVCC. As such, we do not use the main sequence as an absolute definition of the star-forming main sequence for the EVCC sample, but rather as a reference sequence for computing starburstiness. In terms of optical color, RPS class galaxies are overall blue relative to the red sequence, with Class IV galaxies noticeably redder in comparison. As for mid-infrared colors, RPS class galaxies are generally distributed around the star-forming sequence, which indicates that they

are not as quenched in star formation as they may be, as suggested by their star formation rates. This disparity can be explained by the fact that mid-infrared colors trace longer star-forming timescales than those of total IR-derived star formation rates (up to ∼100 Myr; Kennicutt & Evans 2012). Class III and IV galaxies are overall noticeably less star-forming, which is not surprising considering their HI morphology and range of HI deficiencies. In contrast to the clustering of galaxies around the star-forming sequence, we also identify a seemingly passive sequence located around [3.4] − [12] = -2.0. According to Figure 4c from Ko et al. (2013), where they compare their sample of quiescent red sequence galaxies with single stellar population (SSP) models that include mid-infrared emission from AGB stars, the mid-infrared colors of the passive galaxies are roughly consistent with stellar populations with a mean age of $\gtrsim$5 Gyr. Those with [3.4] − [12] $\lesssim$ -2.0 can be described by SSP models without AGB dust. Such galaxies with relatively old stellar populations are found to lie on the optical red sequence and exhibit much lower star formation rates.

We note that RPS class galaxies exhibit different ranges in stellar mass, which shows that there is a need to minimize mass effects. We thus choose to examine the distributions of starburstiness, $\Delta(g - r)$, and $\Delta([3.4] - [12])$. Starburstiness (R_{SB} = $sSFR/sSFR_{MS}$; Elbaz et al. 2011) is a measure of the relative excess of the specific star formation rate (sSFR = SFR/M_*) of a galaxy compared to that of a main sequence star-forming galaxy of the same mass. $\Delta(g - r)$ is a measure of how blue a galaxy is relative to a red sequence galaxy of the same mass, with negative values indicating bluer galaxies and positive values redder galaxies. $\Delta([3.4] - [12])$ measures the deficiency in IR color (which is a proxy for deficiency in star formation) of a galaxy relative to a galaxy of the same mass on the star-forming sequence, with positive values signifying galaxies rich in IR color. Using these parameters thus allows a fair comparison of the star formation tracer distributions between different RPS classes.

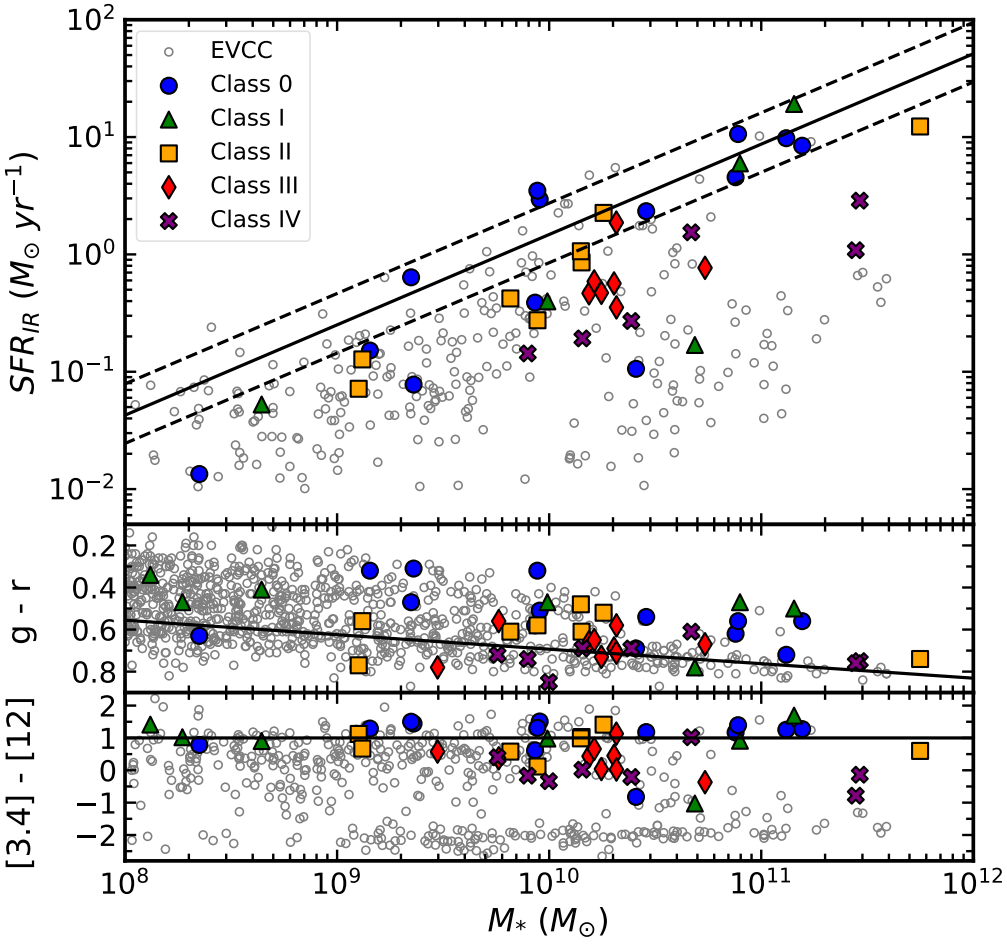

Figure 3.3. Total IR-derived star formation rates, optical, and mid-infrared colors (from top to bottom) as a function of stellar mass for Virgo galaxies with defined RPS classes from Yoon et al. (2017) and the remaining EVCC galaxies with no defined classes plotted as reference. The solid black lines define a reference sequence for each star formation activity tracer, to normalize for the effects of different masses. The reference sequence for SFR_{IR} is the star-forming main sequence defined by Elbaz et al. (2007), and the dashed lines are the lower and upper bounds to the fit. The solid line in the middle panel is the red sequence, which was derived based on a best linear fit of non-RPS Class galaxies with $M_* > 1.5\times10^{10}$ $M_\odot$ and $g - r > 0.58$. The solid line in the bottom panel is adopted from the peak of the mid-infrared color distribution of star-forming galaxies in Hwang et al. (2012b).

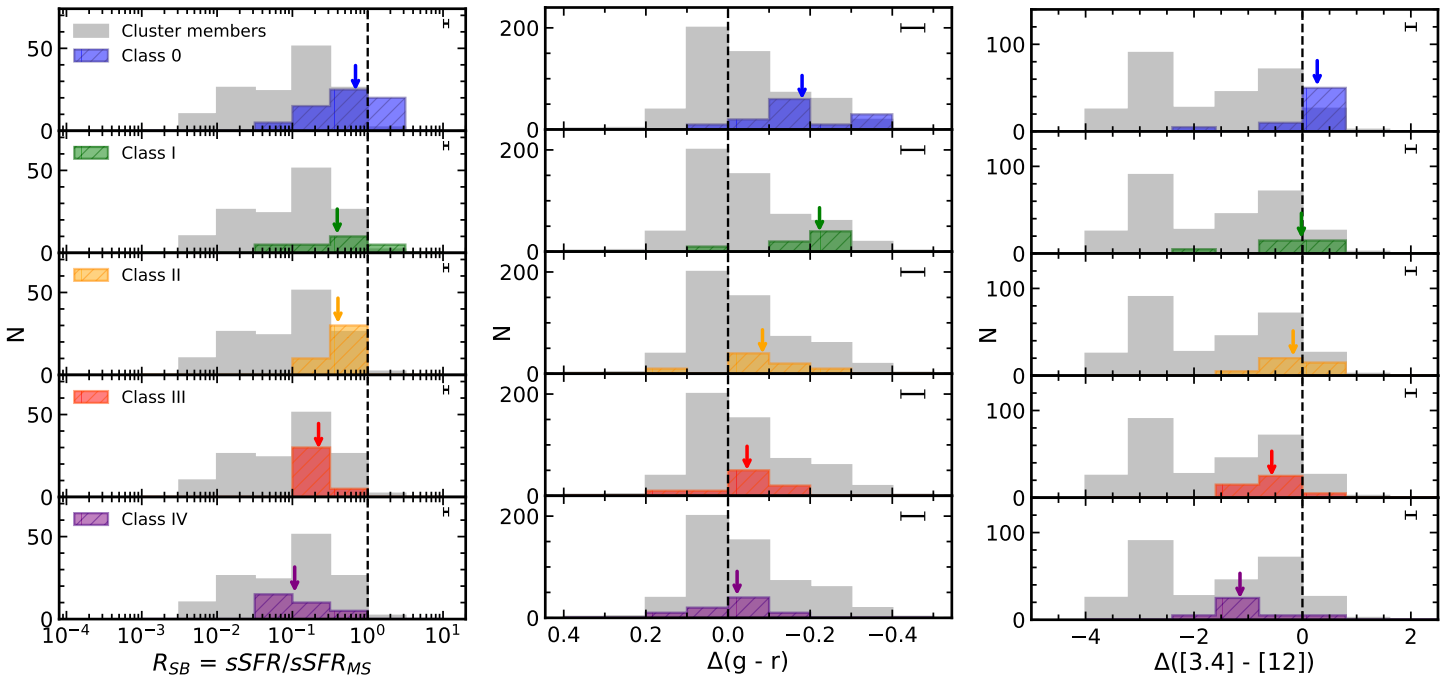

Figure 3.4. Starburstiness (R_{SB}), $\Delta(g-r)$, $\Delta([3.4]-[12])$ histograms (from left to right). Vertical lines denote the locus of the reference sequence (i.e., star-forming main sequence for R_{SB}, red sequence for $g-r$, star-forming sequence for [3.4] − [12]). Certain members, for which cluster membership is given by EVCC, with no defined RPS classifications are plotted together for reference. The arrows represent the median values for each sample. Bin counts were increased by a factor of 5 (10 for the $\Delta(g-r)$ distribution) for RPS galaxies for a fair comparison with the reference sample. The representative (either the mean or the median) errors for each parameter are shown in the top right corner of each panel.

Figure 3.4 shows the resulting histograms of the star formation tracer distributions - starburstiness, $\Delta(g-r)$, and $\Delta([3.4]-[12])$ - from left to right. We denote the median of each distribution with downward arrows. We overlay the distribution of each RPS class on top of that of other cluster members with no RPS classification, as reference. In general, our results show the overall quenching of star formation activity with increasing degree of ram pressure stripping, which agree with the results of previous studies (e.g., Jaffé et al. 2015; Yoon et al. 2017). The resulting distributions of each star formation activity indicator are consistent with one another; we observe an overall decrease in starburstiness, a transition from the blue towards redder colors, and a decline in mid-infrared colors (corresponding to a lower emission in 12μm) with increasing degree of gas stripping. As such, Classes 0 and I make up the actively star-forming end of the cluster population, whereas Classes II and III seem to represent a moderately star-forming population. We also note the presence of galaxies with lower starburstiness and $\Delta([3.4]-[12])$ than RPS class galaxies, which can be attributed to the sequence of quiescent galaxies observed in the bottom panel of Figure 3.3.

While the overall trend of quenching is clear, we are not able to observe any noticeable enhancement in star formation activity for galaxies undergoing early to active stripping, i.e., Classes I and II. There is a hint of a shift in the median of the $\Delta(g-r)$ distribution towards bluer colors for Class I relative to that of Class 0, but given that we are dealing with small number statistics, such a shift seems statistically insignificant. We confirm this by running Kolmogorov-Smirnov (K-S) tests on the RPS class sample. We are not able to reject the hypothesis that the two distributions are drawn from the same population (i.e., the null hypothesis), even at a $>2\sigma$ level, for Classes 0 and I galaxies for any of the star formation activity indicators. Taking into account that the HI deficiency ranges of Class 0 and I galaxies are overall comparable to one another (see Table 3.1), it is not surprising that the distinction between the two classes is statisti-

cally insignificant. Classes I and II also show no statistically significant differences from one another. On the other hand, we are able to reject the null hypothesis for Class 0 and III, and Class 0 and IV at a $>2\sigma$ level for all star formation tracers. The results of the K-S test on the $\Delta([3.4]-[12])$ distribution gives $p_{KS} \approx 0.001$ for Classes 0 and III, and for Classes 0 and IV, indicating a significance of $>3\sigma$. Although there is a trend that the distributions of star formation tracers systematically change with stripping classes, such differences are not strongly supported by statistical tests. We suspect that this is largely due to small number statistics, and the fact that we are using integrated photometry to trace the star formation activity in these galaxies. Moreover, we also consider the possibility that if there is any enhancement in star formation induced by ram pressure stripping, it is unlikely to last for a long enough period of time to be traceable by the star formation tracers used in this study. We discuss the implications of our results in further detail in Section 4. We observe the most statistically significant differences for RPS classes with large disparities in HI deficiencies, relative HI extent, and HI morphology, such as Class 0 and III, and Class 0 and IV.

3.2 Star Formation Properties of Galaxies Classified by HI Mass Fractions and Positions in Phase Space

While we are able to capture the overall quenching of star formation activity with increasing degree of gas stripping with RPS classes, the differences among the stripping classes are not statistically significant. As high-resolution HI imaging is only available for a limited sample of the EVCC, small number statistics do come into play. We thus aim to expand the sample by re-defining new stripping groups using a combination of HI mass fraction (HI mass relative to stellar mass; M_{HI}/M_*) and location in projected phase space. While Yoon et al. (2017) categorized galaxies into different stripping classes

based on HI properties, and then traced the orbital histories of such galaxies using location in projected phase space, we utilize both HI mass fractions and expected position in projected phase space according to radial infall to define a new classification scheme. We visually inspect the EVCC galaxies with HI detections to identify and remove a total of 11 spheroidal galaxies that may have been subject to morphological quenching (Martig et al. 2009) from the sample. This leads to a total of 510 spiral and irregular galaxies with HI detections in the EVCC.

3.2.1 Definition of HI Stripping Groups

To define new HI stripping groups, we first plot the HI mass fraction as a function of stellar mass, and perform a best linear fit of Class 0 and I galaxies to define a reference sequence (Eq. 3.1), as shown in Figure 3.5. Despite differences in HI morphology, Class 0 and I are similar in HI deficiencies (see Table 3.1) and thus the two classes can be thought to represent the HI-rich end of galaxies in the Virgo cluster. As similarly done in Figure 3.4, we measure $\Delta(\log \mathrm{M_{HI}}/\mathrm{M_*})$, the deficiency of the HI mass fraction of a galaxy with respect to that of a galaxy on the reference sequence with the same mass. We then use Gaussian Mixture Modeling (GMM) to identify three groups defined by richness in their HI gas content: HI-normal to rich, HI-poorish, and HI-poor. The GMM results are shown in Figure 3.7. We adopt the intersections of the Gaussian components, i.e., the dashed grey lines in Figure 3.7, as the boundaries between the different groups. The equations defining the ranges of $\Delta(\log \mathrm{M_{HI}}/\mathrm{M_*})$ for each group are given by Eqs. 3.2, 3.3, and 3.4, denoting HI-normal to rich, HI-poorish, and HI-poor, respectively.

$$\log \frac{M_{HI}}{M_*} = -0.919 \log M_* + 8.548 \tag{3.1}$$

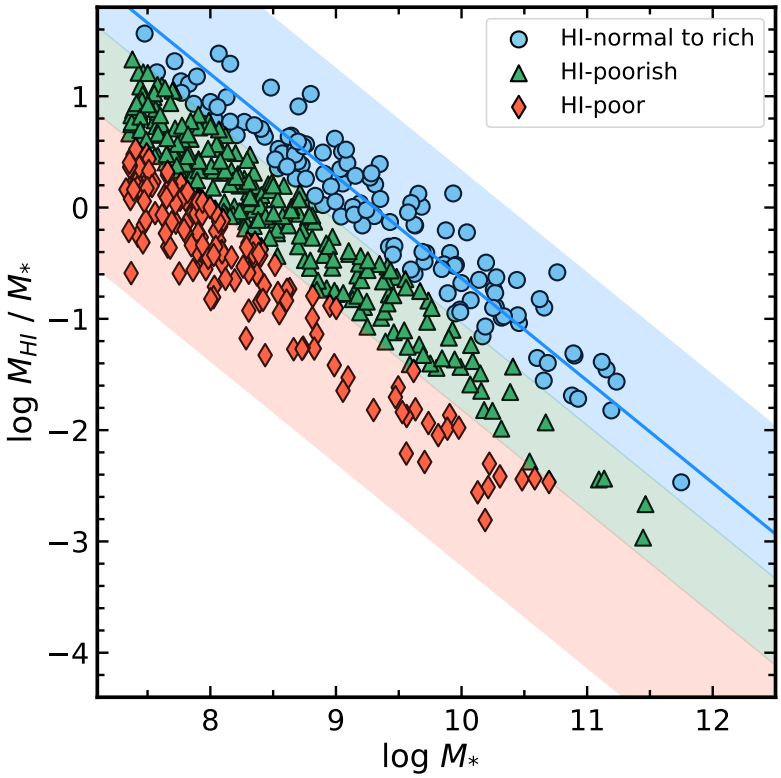

Figure 3.5. HI mass fraction as a function of stellar mass, for which each of the shaded regions mark the range of HI mass fractions of each group, as defined by Eqs. 3.2 through 3.4. The blue line is the reference sequence as defined by a best linear fit of Class 0 and I galaxies, defined by Eq. 3.1.

HI-normal to rich:

$$\log \frac{M_{HI}}{M_*} + 0.919 \log M_* \geq (8.548 - 0.401) \tag{3.2}$$

HI-poorish:

$$\begin{cases} \log \frac{M_{HI}}{M_*} + 0.919 \log M_* < (8.548 - 0.401) \\ \log \frac{M_{HI}}{M_*} + 0.919 \log M_* \geq (8.548 - 1.179) \end{cases} \tag{3.3}$$

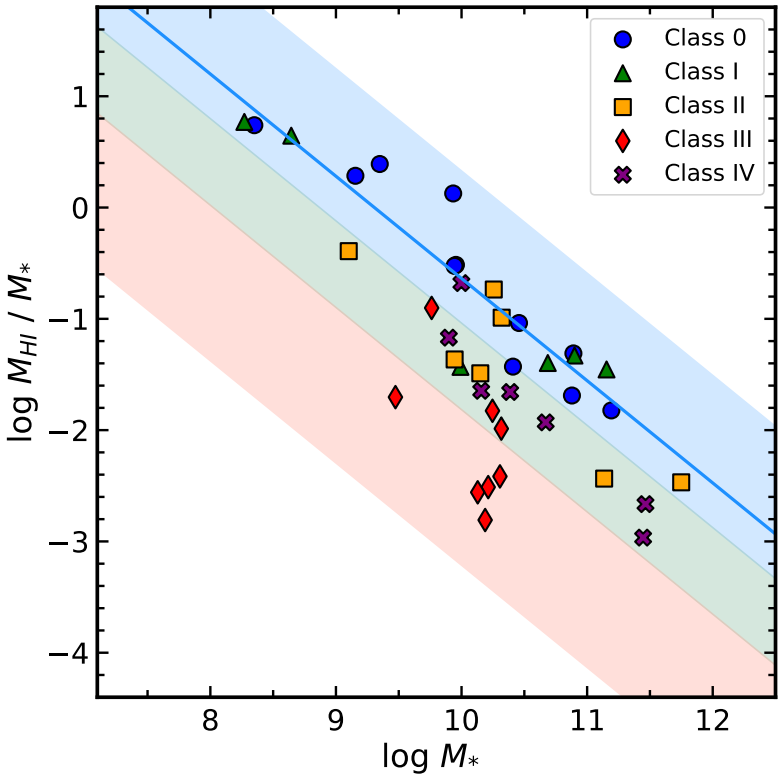

Figure 3.6. HI mass fraction as a function of stellar mass for the RPS class sample, to verify whether the selected ranges of $\Delta(\log M_{HI}/M_*)$ for each group are consistent with those of the RPS class sample.

HI-poor:

$$\log \frac{M_{HI}}{M_*} + 0.919 \log M_* < (8.548 - 1.179) \tag{3.4}$$

With these definitions, we classify galaxies in the EVCC with HI detections into a total of three groups, which are visualized in Figure 3.5. In Figure 3.6, we verify whether the selected ranges of HI mass fractions are consistent with those of the RPS class sample. Despite the presence of some scatter, most of Class 0 and I galaxies are well represented as HI-normal to rich galaxies. The selected range of HI mass fractions

for the HI-poorish group is consistent with those of Class II and III galaxies, and we confirm that more than half of the Class III objects are categorized as HI-poor galaxies. With the exception of one galaxy, Class IV galaxies are generally well described as HI-poorish, which is expected given that their HI deficiency range overlaps with that of Class II galaxies (see Table 3.1). We thus affirm that the selected ranges of $\Delta(\log M_{HI}/M_*)$ for each group, as given by the results of GMM, are well founded.

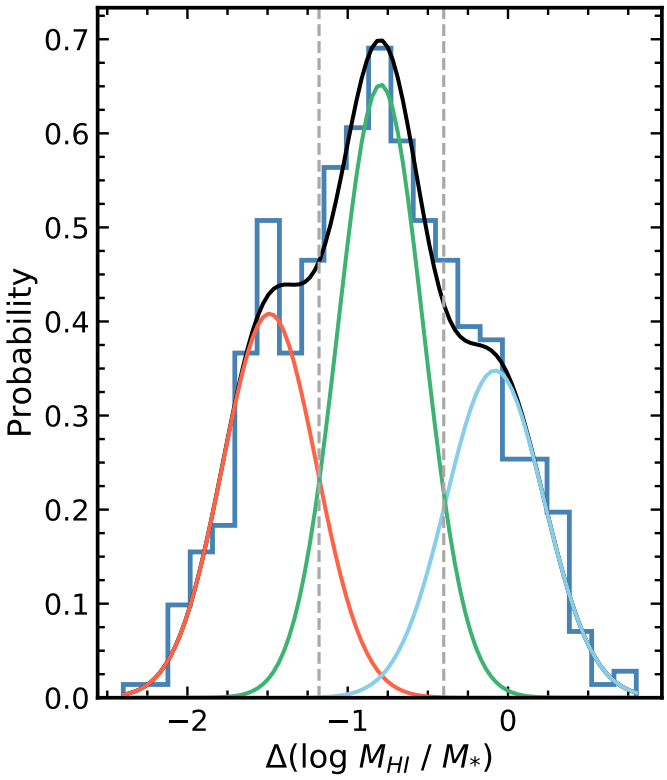

Figure 3.7. $\Delta(\log M_{HI}/M_*)$ histogram with the resulting Gaussian Mixture Model (GMM) overlaid on top. Each Gaussian component specifies the mean and range of a potential HI group. The blue component represents the HI-normal to rich galaxies, the green represents the HI-poorish galaxies, and the red the HI-poor. The grey dashed lines mark the intersections between the different Gaussian components.

To distinguish galaxies at different stages in their orbital histories, we employ the use of projected phase space as a second means of categorizing galaxies into HI stripping groups, as shown in Figure 3.8. We utilize the same definitions of regions in phase space as shown in Figure 3.1. Galaxies that are likely to be on their first infall are expected to be found in Region A. For those that are approaching their first core crossing, or have already passed and are falling out of the core, they are likely to be found in Region B. Galaxies that have gone through multiple core crossings will eventually settle and virialize within the cluster potential, finding themselves at low velocities and clustercentric distances, such as Regions C or D. However, as confirmed by Yoon et al. (2017), it is possible that some galaxies may reach further out after outfall, otherwise known as backsplashing galaxies. We briefly examine the possibility of finding backsplashing candidates with our group categorization in Section 4.2.2. As for galaxies that are located at relatively high velocities and large clustercentric distances, they are less subject to the cluster potential and thus are expected to retain a comparable amount of HI mass as that of a field galaxy. We may find such galaxies in Region E. However, we stress that the HI-normal to rich galaxies located in Region E are not an ideal control sample of galaxies outside of the cluster potential well, as those presumed to be background galaxies were excluded from the EVCC with a radial velocity cut, as mentioned in Section 2. We finalize our HI group sample based on their expected position in phase space, in combination with their HI mass fractions, resulting in a total of 241 galaxies. The final HI group sample is presented in Table 3.2, labeled as HI-normal-E, HI-poorish-AB, and HI-poor-BCD. Amongst the final sample, there is a total of 16 galaxies that comprise the RPS class sample in Yoon et al. (2017). There are 11 galaxies categorized as HI-poorish-AB, which consist of a mixture of Classes 0 - IV. The HI-poor-BCD group consists of 4 Class III galaxies. The remaining galaxy is one of the confirmed backsplashing candidates in Yoon et al. (2017).

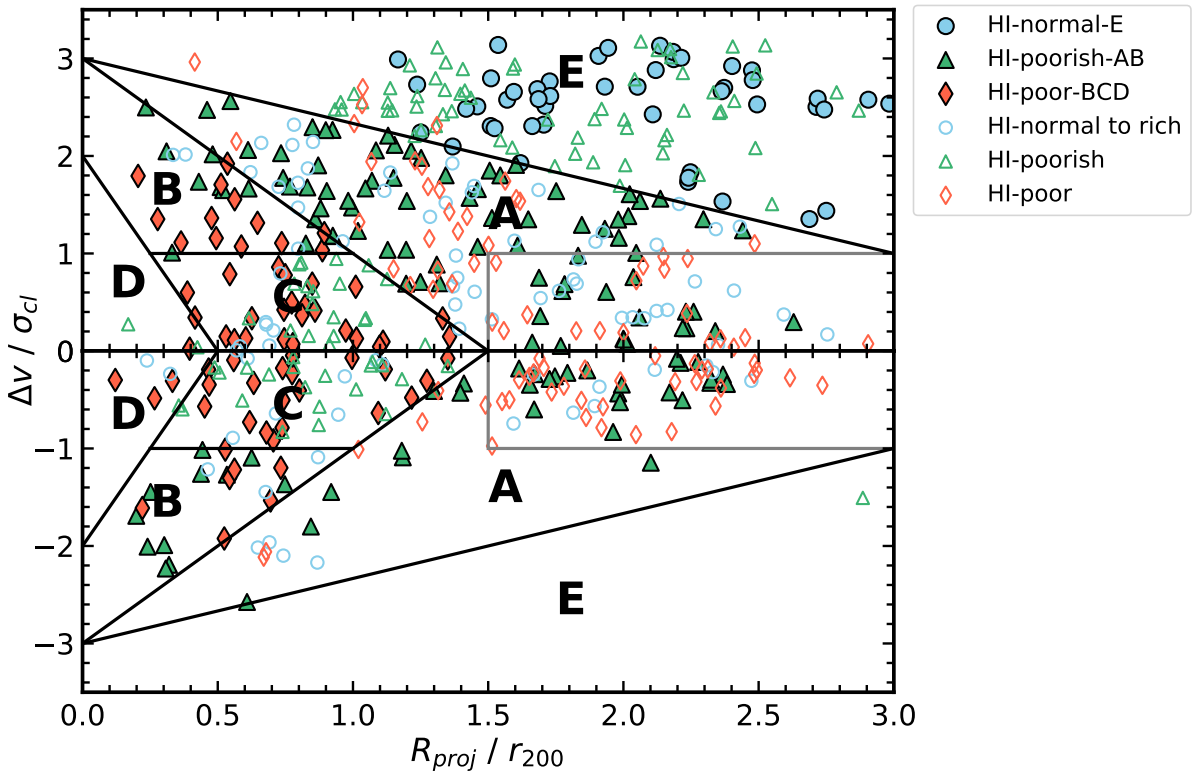

Figure 3.8. Projected phase-space diagram of all newly defined HI stripping groups. The black solid lines indicate the boundaries between different regions of time since infall as shown in Figure 3.1. The final group candidates are shown as filled color symbols, whereas those that did not satisfy the condition of expected location in phase space are shown as open symbols. Red open symbols (HI-poor galaxies located outside of Regions B through D) residing in the region defined by grey solid lines are selected as potential backsplashing candidates, which are discussed briefly in Section 4.2.2.

Table 3.2. Categorization of the EVCC into different HI stripping groups

HI Stripping Group	$\Delta(\log M_{HI}/M_*)$ (Range)	Location in phase space
(1)	(2)	(3)
HI-normal-E (N = 48)	Eqn. 3.2	Region E
HI-poorish-AB (N = 125)	Eqn. 3.3	Regions A or B
HI-poor-BCD (N = 68)	Eqn. 3.4	Regions B, C, or D

(1) HI stripping group, (2) HI mass fraction range, and (3) location in phase space.

When plotting the projected phase-space diagram, we take on the same assumptions as done in Yoon et al. (2017). Here, we assume that the center of the Virgo cluster is at M87 (Böhringer et al. 1994). We normalize the projected clustercentric distance by r_{200} and the line-of-sight clustercentric velocity by the cluster dispersion, σ_{cl}. The clustercentric velocity is calculated using the difference between a galaxy's velocity along the line-of-sight and the mean radial velocity of the M87 subgroup, 1088 km s^{-1} (Cluster A; Mei et al. 2007). We adopt values of r_{200} = 1.55 Mpc (McLaughlin 1999; Ferrarese et al. 2012) and σ_{cl} = 593 km s^{-1} (Mei et al. 2007).

3.2.2 Star Formation Properties of New HI Stripping Groups

We examine the star formation properties of the newly defined HI stripping groups, using a much more statistically significant sample. Using the same star formation tracers as before, we show our results in Figure 3.9. As seen similarly with Figure 3.3, we are

not able to observe a specific trend in the HI stripping groups, especially given that a disparity in the range of stellar mass is apparent between them. For example, a large fraction of HI-poorish-AB and HI-poor-BCD galaxies appear to dominate the low-mass end, whereas the high-mass end seems to be increasingly dominated by HI-normal-E galaxies. As such, we perform the same in-depth analysis as done in Section 3.1.2, where we minimize biases due to mass effects by plotting the histograms of starburstiness, $\Delta(g - r)$, and $\Delta([3.4] - [12])$. Moreover, for a fair comparison between the distributions of different star formation tracers, we perform a stellar mass cut of $2{\times}10^8$ $M_\odot \leq M_* \leq 4{\times}10^{10}$ $M_\odot$, which is roughly the stellar mass range of galaxies with measured SFR_{IR} (as plotted in the top panel of Figure 3.9), excluding a select few outliers on the high-mass end.

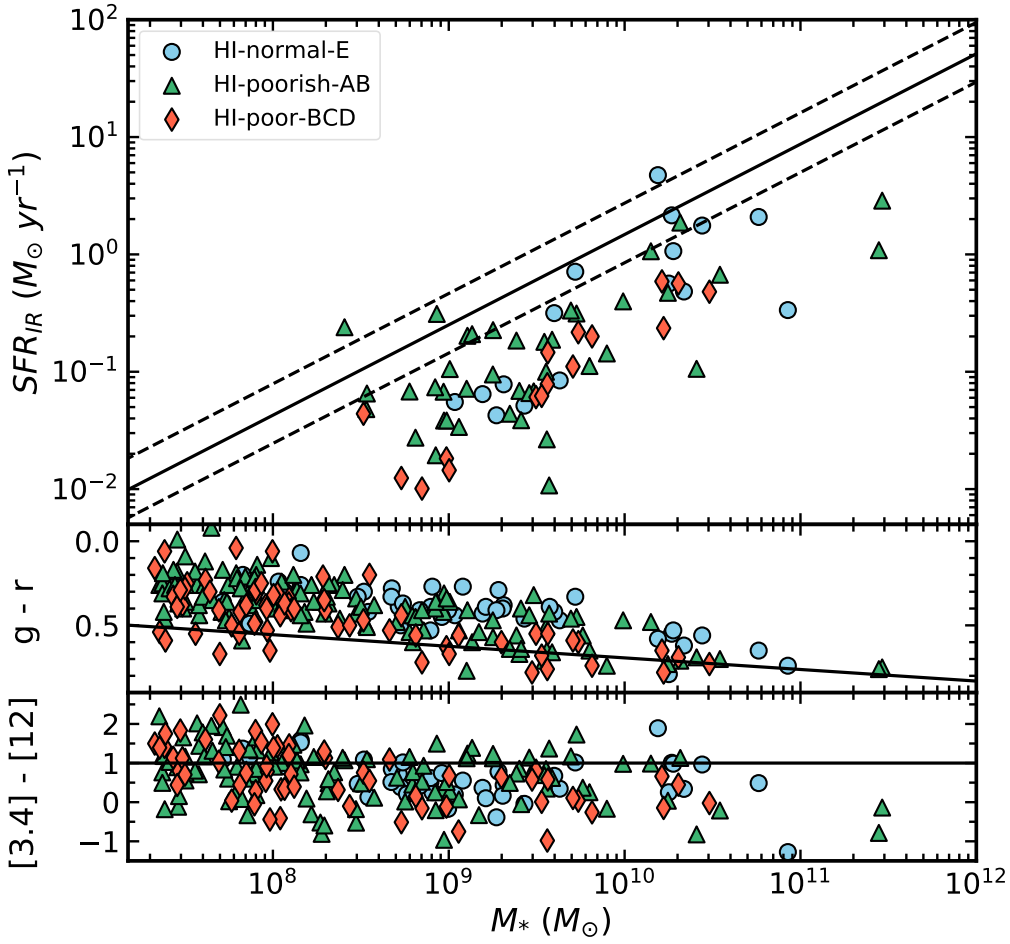

Figure 3.9. Star formation rates derived from total IR luminosities, optical, and mid-infrared colors (from top to bottom) as a function of stellar mass for the EVCC sample with newly defined HI stripping groups. The reference sequences shown here are identical to the ones used in Figure 3.3.

The resulting histograms are shown in Figure 3.10. We observe an overall decrease of starburstiness with decreasing HI gas content, which is consistent with the results shown in Figure 3.4. The starburstiness distribution shows that the median values are nearly equal for HI-normal-E and HI-poorish-AB groups, while the median of the HI-poor-BCD group is shifted towards lower values of R_{SB}, the latter of which agrees with our expectations and previous results in Section 3.1.2. However, K-S tests on the starburstiness distributions yield far less than significant results, all giving $p_{KS} > 0.05$. We believe this may be due to the fact that the *WISE* 22μm detection limit is not deep enough to result in a large sample of galaxies compared to those of other star formation tracers. On the other hand, we see a much clearer trend in the change in star formation activity for $\Delta(g - r)$; the median $\Delta(g - r)$ increases towards redder colors with decreasing HI gas content. Our K-S test results give a p-value of less than $\sim$0.05 for HI-normal-E and HI-poorish-AB galaxies. We are also able to reject the null hypothesis at a $> 3\sigma$ level for HI-normal-E and HI-poor-BCD galaxies, and HI-poorish-AB and HI-poor-BCD galaxies. In contrast, we observe slightly different results with the $\Delta([3.4] - [12])$ distribution. There is an apparent shift in the median $\Delta([3.4] - [12])$ towards larger values, indicating an enhancement of star formation activity in HI-poorish-AB galaxies, relative to that of HI-normal-E galaxies. We then observe a quenching of the star formation activity of HI-poor-BCD galaxies with the median shifted towards negative values of $\Delta([3.4] - [12])$. However, the supposed enhancement of star formation activity observed by the shift in the median is not expected to be meaningful as the K-S test does not yield significant results and the difference in the median values are only slightly out of the range of error. On the other hand, we observe a statistically significant difference between HI-normal -E and HI-poor-BCD galaxies, and HI-poorish-AB and HI-poor-BCD galaxies with a p-value < 0.02 for both. In general, our results suggest that there is no statistically significant difference between HI-normal-E and

HI-poorish-AB galaxies. However, we are able to reject the null hypothesis at a $>2\sigma$ level for the optical color distribution. We also observe a significant difference between HI-poorish-AB and HI-poor-BCD galaxies for all star formation tracers. Overall, we are able to capture the quenching of star formation activity with increasing deficiency in HI gas content with a statistically significant sample compared to our analysis in Section 3.1.2.

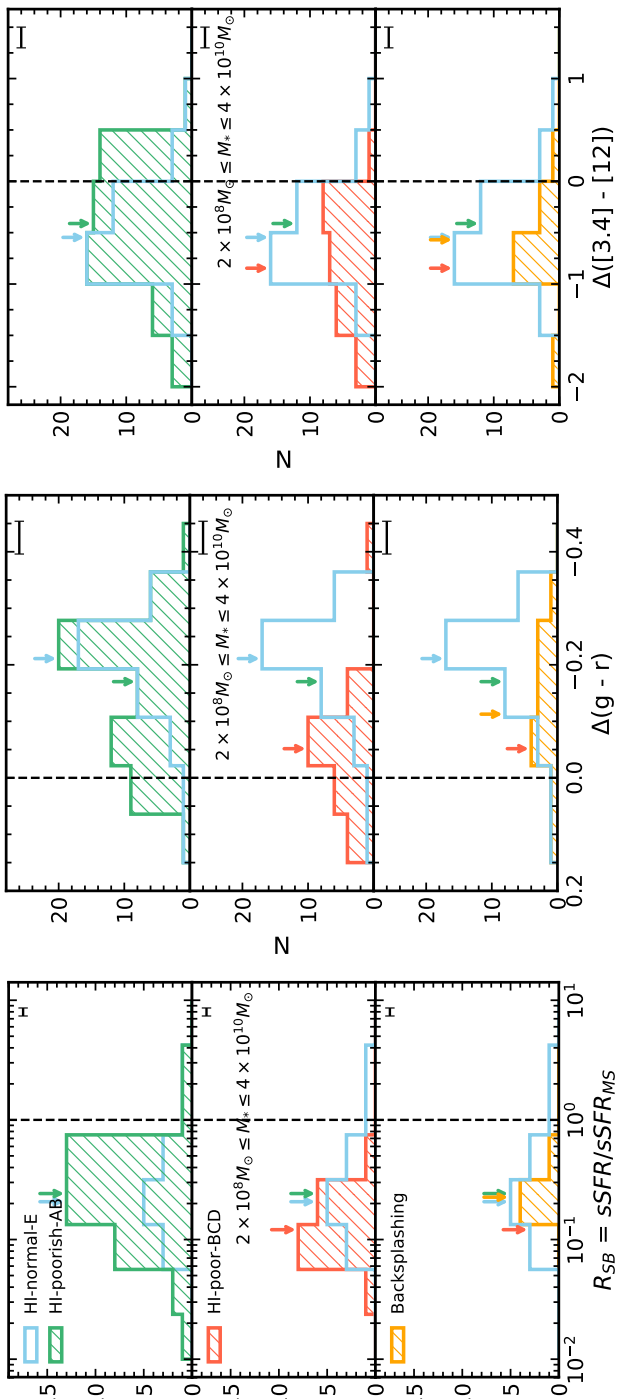

Figure 3.10. Starburstiness (R_{SB}), $\Delta(g-r)$, $\Delta([3.4]-[12])$ histograms (from left to right) for new HI stripping groups. The downward arrows mark the median of each distribution. The vertical lines here are the same lines defined in Figure 3.4. Stellar mass range of the subsamples used are displayed in the middle panel of each histogram. Additionally, we show the distribution of potential backsplashing candidates in the bottom panel.

Chapter 4

Discussion

4.1 Locally Enhanced Star Formation in Galaxies Undergoing Gas Stripping

We examine the star formation activity of galaxies undergoing ram pressure stripping in the Virgo cluster using various tracers. We initially perform a follow-up study of Yoon et al. (2017), given the availability of high-resolution HI-imaging thanks to the VIVA survey (Chung et al. 2009). While our results confirm the previously known trend of star formation quenching with increasing degree of ram pressure stripping (Jaffé et al. 2015; Yoon et al. 2017), the difference between the distributions of galaxies undergoing early through post stripping is not statistically significant. However, we do observe a statistically significant distinction between Class 0 and III, and Class 0 and IV galaxies.

4.1.1 Implications from Observational Studies Based on the Virgo Cluster

The lack of a conspicuous enhancement in star formation activity is not too surprising given the results of previous studies on the Virgo cluster. Koopmann & Kenney (2004b)

utilize the spatial distributions of Hα and R-band emission to investigate the environmental effects on the star formation activity on 52 galaxies in the Virgo cluster, among which 39 of them are RPS class galaxies. Most of the Hα-truncated spirals show signs of having been subject to ram pressure stripping, where many of them exhibit normal to slightly enhanced star formation rates in the inner galaxy disks. While they find asymmetric enhancements in star formation at the outer edge of the Hα disk for a few galaxies, including NGC 4654 (Class II) and NGC 4405 (Class III), which is indicative of ongoing ICM pressure, these enhancements are at most globally modest and local. They instead find that galaxies with the largest global enhancement in star formation are those that have undergone low-velocity tidal interactions and/or gas accretion. An example of such a galaxy in their sample is NGC 4299 (Class I), which shows evidence of undergoing both RPS and tidal interactions due to its pair galaxy NGC 4294 (Class I). Furthermore, pixel-by-pixel analyses of FUV images by Boissier et al. (2012) show little to no star formation activity in the stripped HI gas of a select few Class I and II galaxies, with NGC 4522 (Class II) being an exception. However, the authors come to the conclusion that despite the presence of a mild enhancement in star formation, it is unlikely to affect the global star formation activity and thus will not be discernible when considering integrated quantities or large samples of galaxies as a whole. As RPS class galaxies show to be undergoing quenching on a global scale as a result of ongoing gas stripping, any local enhancement in star formation is unlikely to be discernible with integrated photometry. This explains why, on top of small number statistics, the differences in star formation activity between different RPS classes are not statistically significant.

On the other hand, we observe a significant difference on a $>3\sigma$ level between Classes 0 and III, and Classes 0 and IV. Use of integrated photometry works particularly well in cases where galaxies showing large disparities in HI gas content and star formation

activity are compared with one another. Moreover, Yoon et al. (2017) suggest that Class IV galaxies are likely to have undergone starvation (Larson et al. 1980), given that they show gas depletion at all radii in the disk instead of the expected asymmetry arising from ram pressure stripping in their HI morphology. Such galaxies would have their star formation quenched throughout the disk, which would be apparent when traced with integrated properties.

While enhancements in star formation may be prominent for galaxies undergoing gas stripping in other galaxy clusters (e.g., Vulcani et al. 2018; Ramatsoku et al. 2019), it is evident that the data used in this study do not show such a global enhancement for galaxies in the Virgo cluster. If one intends to capture the local enhancement of star formation in Virgo galaxies, spatially resolved data would be necessary, as done in Koopmann & Kenney (2004b). Results of Lee et al. (2017) further prove the advantage of using spatially resolved data - they confirm strong enhancement in both far-ultraviolet (FUV) and Hα along CO compression within the stellar disk for three Class II galaxies, which support our hypothesis that galaxies undergoing active stripping are likely to experience some sort of star formation enhancement. Boselli et al. (2018) take advantage of deep narrow-band Hα+[NII] imaging of NGC 4254 (Class I) to find $\sim$60 compact star-forming regions located along the stripped HI gas tail, implying that star formation had been triggered by ram pressure stripping.

In addition, Kenney et al. (2014) suggests that whereas galaxies with one-sided tails of young stellar knots are often observed in more distant and massive (i.e., denser ICM and higher peak ram and thermal pressures) clusters such as the Coma cluster, the Virgo cluster itself is not massive enough to completely strip spiral galaxies. However, such features can be observed in lower mass galaxies such as dwarf irregulars, as Kenney et al. (2014) show with their analysis of IC 3418. IC 3418 was not included in the EVCC, and moreover has been shown to have weak HI (Chung et al. 2009; Kenney et al. 2014)

and mid-infrared emission (checked with *WISE* 12μm and 22μm images). Thus, our overall results are unlikely to have changed significantly even if we had included dwarf irregular galaxies such as IC 3418, given our choice of star formation tracers.

4.1.2 Impact of RPS on the Global Star Formation Activity of Galaxies as Predicted by Simulations

Results of previous observational studies, along with ours, suggest that a global enhancement in star formation triggered by RPS is rather mild and challenging to detect when considering integrated quantities or large samples of galaxies as a whole. Studies such as Kenney et al. (2014) suggest that the degree of enhancement depends on a variety of factors, such as the stellar mass of the galaxy, total mass of the host galaxy cluster, density of the ICM, etc. Moreover, recent simulation studies (e.g., Oman & Hudson 2016; Rhee et al. 2017) tracing the trajectories of infalling cluster galaxies in phase space have shown that the relative velocity of galaxies, along with the ambient ICM density, changes with the galaxy's location with respect to the cluster center. As such, the impact of RPS on the star formation activity is not a trivial matter, given that it is also closely coupled with the orbital history of the galaxy.

Disagreements with regards to the degree or even the possibility of global enhancement are also found in simulation studies, given the strong dependency on initial conditions. Kronberger et al. (2008) and Kapferer et al. (2009) report that the total SFR is predicted to be significantly enhanced for factors of $3 \sim 10$ by ram pressure, compared to the same galaxy evolving in isolation. In contrast, recent RPS simulations such as Bekki (2014) and Steinhauser et al. (2016) suggest that global enhancement of star formation induced by ram pressure is modest at best (e.g., not on the order of a factor of $\sim$10). Understanding the discrepancies between the results of these studies requires looking into differences in the simulation setups. Because Kronberger et

al. (2008) and Kapferer et al. (2009) both implement simplified models of a galaxy moving at a constant velocity through a homogeneous ICM, it is advised to take their results with a grain of salt. On the other hand, Bekki (2014) and Steinhauser et al. (2016) model galaxies of different stellar masses subject to a time-variable ram pressure as they infall towards the cluster core. Moreover, they also model environments with a range of masses (from group-like, Virgo-like, to Coma-like clusters) and allow their model galaxies to undergo different orbital trajectories. As such, their results show to be more credible compared to simplistic wind-tunnel simulations of RPS. However, while both Bekki (2014) and Steinhauser et al. (2016) agree on the feasibility of a modest enhancement of star formation on global scales, they disagree with one another in the required conditions for enhancement to occur. For example, while Bekki (2014) find that global enhancement can be seen in Milky Way (MW)-like disk galaxies ($M_{disk,*} \sim 5.4{\times}10^{10}$ $M_{\odot}$) in Virgo-like clusters, but not in Coma-like clusters, Steinhauser et al. (2016) report the contrary - ram pressure only leads to continuous stripping for MW-like galaxies in Virgo-like clusters, leading to minor effects on the SFR. The differences in these results once again stem from simulation setups - upon comparison of orbital pericenter, Bekki (2014) allows a very close approach of $d_{center} \sim 0.03\ r_{200}$, whereas in Steinhauser et al. (2016)'s simulation, the galaxy travels down to $\sim$0.74 r_{200} before falling back out towards the outskirts. Given that ram pressure is expected to be highest at the cluster center, the difference in the results of Bekki (2014) and Steinhauser et al. (2016) seem to arise from the implementation of different orbital trajectories and consequently different pericentric distances. Overall, simulation results by Bekki (2014) and Steinhauser et al. (2016) show that modest global enhancement takes place under rather rigorous conditions. As such, the number of galaxies undergoing enhancement likely make up a small fraction of the cluster population, making it less distinguishable when considering the cluster population as a whole.

Just as galaxies undergoing even a modest degree of global enhancement can be rare in galaxy clusters, as insinuated by recent simulation studies, it is also worthwhile exploring the possibility that the enhancement timescale is rather short, which may bring the choice of star formation tracers used in this study into question. There is no clear consensus with regards to the timescale over which enhancement lasts as reported by simulation studies, just as there is none with regards to the degree of global enhancement. Kronberger et al. (2008) report that the SFR is always significantly higher compared to that of an isolated galaxy over 500 Myr, whereas Kapferer et al. (2009) seem to suggest that the enhancement timescale depends on the strength of ram pressure and the density of the surrounding gas. The stronger the ram pressure, the shorter the timescale of enhancement, as they report a timescale of $<$80 Myr in their simulation run with the highest ram pressure. On the other hand, Bekki (2014) and Steinhauser et al. (2016) do not mention a particular timescale, in fact, their results show that the timescale of enhancement shows to vary depending on the galaxy's mass, orbital trajectory, along with the host cluster mass.

Despite discrepancies in simulation results with regards to enhancement timescales, one could nevertheless try to constrain the time period for which the enhancement stage can be best captured. Given that the compression of interstellar gas due to ram pressure is expected to be strongest at orbital pericenter (e.g., Vollmer 2009; Bekki 2014), it would be reasonable to assume that a modest starburst could occur around this stage of a galaxy's orbital history. Using models based on galaxies in the Virgo cluster, Vollmer (2009) claims that the time window during which one could identify perturbations due to RPS around peak ram pressure is $\sim$300 Myr. With this in mind, RPS itself is expected to occur on a relatively short timescale of 100 Myr (e.g., Roediger 2009). SFRs based on TIR luminosities are sensitive to timescales of $\sim$100 Myr (Kennicutt & Evans 2012), which implies that our choice of star formation tracers was appropriate. However,

it is entirely possible that any enhancement due to RPS may occur for even shorter timescales, such that it would be more advantageous to use star formation tracers sensitive to even shorter timescales (∼10 Myr), such as Hα. Barring that possibility, our choice of star formation tracers do not seem to be of an issue in terms of sensitivity to star formation timescales.

It is also worth noting that previous studies have found that while RPS can enhance the global SFR for albeit a short period of time, such changes were not discernible in galaxy colors. For example, Fujita & Nagashima (1999) study the change in the SFR along with a galaxy's optical $B - V$ color to find that while the SFR increases by at most a factor of 2, the color stays overall the same. The authors suggest that ram pressure compression does not induce observable star formation activity as the intrinsic scatters of color and luminosity among galaxies are larger. In fact, after stripping occurs, the color of their model galaxy rapidly turns red. Kapferer et al. (2009) also report similar results, in that despite significant enhancement of the overall SFR due to ram pressure, a blue star-forming disk galaxy is expected to transform into a red, passively evolving system under <250 Myr. Steinhauser et al. (2016) studied the SDSS $u - i$ color evolution of their model galaxies to find similar results as well, with the rate of evolution towards redder colors dependent on the strength of ram pressure. As such, while it is feasible to trace the overall quenching of star formation activity with galaxy colors, results of previous studies seem to suggest that galaxy colors are not sensitive to short-term enhancements of the SFR.

4.2 Depletion of HI Gas Content According to Time Since Infall in Phase Space

As the RPS classification given in Yoon et al. (2017) is limited to galaxies with high-resolution HI imaging, we build a more statistically significant sample of galaxies undergoing ram pressure stripping in the cluster by using a combination of HI mass fractions and positions in projected phase space. We examine a total of three different groups of galaxies in the EVCC, with the final sample totaling to 241: 1) HI-normal-E: HI-normal to rich galaxies located at large clustercentric distances and high velocities, 2) HI-poorish-AB: HI-poorish galaxies likely to be on their first infall into the cluster core, and 3) HI-poor-BCD: HI-poor galaxies that are in the process of virializing within the cluster core.

4.2.1 Overall Quenching of Star Formation with Decreasing HI Gas Content and Increasing Time Since Infall

Given the disparity in HI gas content and location in projected phase space, one may expect to see relatively quenched star formation in HI-poorish-AB galaxies compared to that of the HI-normal-E galaxies. However, as mentioned in Section 3.2.2, the two groups are not necessarily distinct from one another. While the distribution of the star formation properties of HI-poorish-AB galaxies does insinuate that they are starting to become quenched (or even undergo a slight enhancement in star formation prior to being quenched), the results of the K-S test indicate that this distinction is most likely negligible. One possible explanation for the lack of a significant discrepancy is that while it is expected for HI-poorish-AB galaxies to become quenched as they infall into the cluster core, the number of galaxies that have actually begun quenching may not comprise of a large fraction of the group. In fact, while HI-poorish-AB galaxies are likely

to have begun losing their gas due to the ICM, the effects of gas loss could have yet to be reflected in the tracers of star formation activity used in this study. If the latter is true, then it is not surprising that the star formation activity of HI-poorish-AB and HI-normal-E galaxies are hardly distinguishable from one another. Simulation results reported in Oman & Hudson (2016) suggest that star formation quenching occurs after a delay time of typically 3.5 - 5 Gyr, measured from the first crossing of 2.5 r_{vir}, roughly equivalent to 3.4 r_{200}. This usually corresponds to times near or shortly after first pericentric approach. As a significant fraction of HI-poorish-AB galaxies still have yet to make their first pericentric passage, it is likely that they have yet to have their star formation quenched, which can explain the lack of discrepancy in their star formation activity with that of HI-normal-E galaxies. On the other hand, we are able to confirm with a $>2\sigma$ confidence that HI-poor-BCD galaxies are likely to be at a different stage in their orbital histories and thus are a distinct population of galaxies within the Virgo cluster, compared to HI-normal-E and HI-poorish-AB galaxies.

While we defined sharp boundaries between different regions in projected phase space, categorized according to time since infall as shown by the simulation results of Rhee et al. (2017), we stress that the locus of these boundary lines are not to be taken as absolute dividing lines between distinct populations of galaxies in phase space. They are merely to be used as a means of identifying galaxies likely to be undergoing ram pressure stripping given their HI gas fractions in projected phase space. To confirm that our results are not significantly affected by the locus of the boundary lines in phase space, we perform tests by making different modifications to the boundaries. For example, we have tried lowering the upper limit of the boundary line of Region E from $\Delta v/\sigma_{cl} = 3$ to 2.5, which allowed an increase in the selection of HI-normal-E galaxies. We also tightened the selection of HI-poor-BCD galaxies by limiting Regions B and C to lower velocities and clustercentric distances. In spite of these alterations, there were

no significant changes observable in the star formation distributions. We thus confirm that our results are not significantly changed even if we make different modifications to the boundaries of different regions in phase space.

4.2.2 Potential Backsplashing Population

We also examine a potential backsplashing population of galaxies in the Virgo cluster. The existence of a backsplashing population in the outskirts of galaxy clusters has long been discussed since Balogh et al. (2000) and Mamon et al. (2004). After the first core crossing, galaxies may travel out as far as 2.5 times the virial radius of the cluster (Gill et al. 2005). Such galaxies are then expected to make another subsequent infall into the cluster core, eventually joining the galaxies that are virializing in the cluster core. We select a potential group of backsplashers by choosing HI-poor galaxies residing in the region $|\Delta v| / \sigma_{cl} \leq 1$ and $R_{proj}/r_{200} \geq 1.5$, resulting in a total of 49 galaxies (refer to Figure 3.8). Amongst the selected candidates, there is one Class III galaxy present, NGC 4064, which was confirmed as a backsplasher in Yoon et al. (2017). Yoon et al. identified a total of four backsplashing galaxies in projected phase space, of which NGC 4457 is classified as HI-poorish-AB, NGC 4580 is HI-poor-BCD and does not fall within the selected region of backsplashing candidates, and NGC 4293 has no measured HI mass given by ALFALFA. The confirmed backsplashing candidates in Yoon et al. (2017) are Class III galaxies located near $\Delta v/\sigma_{cl} \sim 0$ and at roughly 1.2 - 1.7 r_{200} in Figure 3.2. Compared to these galaxies, we have chosen a sample of backsplashing candidates that are overall travelling at relatively larger velocities with respect to the cluster, and some are found even further out to the outskirts around 2.5 - 3 r_{200}. We examine the star formation activity of these candidates in comparison to the three HI stripping groups. We show the resulting distributions of each star formation tracer in the bottom panels of Figure 3.10. We perform the same stellar mass cut for each star formation tracer as

described in Section 3.2.2 for consistency.

Overall, the selected backsplashing group seems to represent an intermediate population between HI-poorish-AB and HI-poor-BCD galaxies. Taking into account that backsplashing may occur past the cluster's virial radius after first core passage, the trend seen in Figure 3.10 seems to make sense. Although the trend seen in the starburstiness distribution is unclear due to the limited number of galaxies with SFR estimates (i.e., *WISE* 22μm detections), we are able to observe increased star formation quenching as a galaxy makes multiple pericentric approaches within the Virgo cluster. If they are true backsplashers, we surmise that they will eventually join the HI-poor-BCD galaxies near the cluster core, and become passive as they continue to lose their gas. We also consider the possibility that these galaxies may not be a true backsplashing population, and may very well have lost their gas through means other than ram pressure stripping. When galaxies are accreted into a nearby galaxy cluster, some may fall in as an isolated galaxy, but it is also likely that a significant fraction of them may fall in as a group. Simulation results of McGee et al. (2009) show that a $10^{14.5}$ h^{-1} $M_{\odot}$ cluster at z = 0 has accreted about 40% of its galaxies ($M_{*} > 10^{9}$ h^{-1} $M_{\odot}$) from groups with masses greater than 10^{13} h^{-1} $M_{\odot}$. Prior to infall, galaxies in groups are likely to have their star formation quenched due to mechanisms such as galaxy-galaxy interactions and galaxy-group tidal interactions, a phenomenon known as "pre-processing" (Fujita 2004). These galaxies thus may appear to have lost even more gas with respect to their location in projected phase space. Taking into account the presence of filamentary structures such as the Leo II A and B filaments (Kim et al. 2016) around the vicinity of the Virgo cluster, pre-processing is definitely a possibility that we cannot rule out when it comes to interpreting the gas content of galaxies in projected phase space.

Chapter 5

Summary & Conclusions

We investigate the star formation properties of galaxies undergoing ram pressure stripping in the Virgo cluster, building upon the analysis of the orbital histories of VIVA galaxies with high-resolution HI imaging as reported in Yoon et al. (2017). We use starburstiness, optical, and mid-infrared colors to examine the star formation activity of galaxies undergoing different stages of ram pressure stripping. Due to the limited number of galaxies with high-resolution HI imaging, we extend our study to the EVCC sample using HI mass fraction and position in projected phase space to categorize galaxies into different stages of stripping. We summarize our main results below.

1. We identify a trend of decreasing star formation activity with increasing degree of stripping, as confirmed by previous studies. However, we do not find strong evidence for star formation enhancement in galaxies undergoing early through active stripping. We attribute the lack of a strong discernment towards the insensitivity of integrated photometry towards local star formation enhancements and the possibility of a relatively short enhancement stage.

2. To make up for the shortcomings of small number statistics, we extend our study towards the EVCC sample, using HI mass fractions and position in projected

phase space. We identify three HI stripping groups - HI-normal to rich, HI-poorish, and HI-poor - represented by different ranges of HI mass fractions. We then perform a second means of categorization by expected location in projected phase space according to radial infall into the cluster core.

3. While we are not able to observe a strong discernment in the star formation properties between the HI-normal-E and HI-poorish-AB groups, the HI-poor-BCD group shows to be clearly quenched in star formation with respect to the other two groups. We attribute the lack of an obvious distinction between HI-normal-E and HI-poorish-AB galaxies to the late onset of star formation quenching.

4. We investigate a potential backsplashing population, selected from HI-poor galaxies located at low velocities and large clustercentric distances beyond the virial radius of the cluster. Distributions of their star formation activity show that they may represent an intermediate population between HI-poorish-AB and HI-poor-BCD galaxies. We also do not rule out the possibility that these galaxies might have lost their gas through pre-processing rather than ram pressure stripping.

We utilized the availability of multi-wavelength data for galaxies in the Virgo cluster to study the star formation properties tracing different timescales. However, the parameters we extracted were based on integrated photometry, which limited a detailed study of the effects of ram pressure stripping on the ISM of the galaxies. To study the comprehensive picture of ram pressure stripping on the star formation activity of cluster galaxies, it is needed to make use of high spatial resolution data obtainable via integral field spectroscopy (IFS) observations. IFS data allows spatially resolved mapping of emission lines from which one can obtain diagnostic line ratios to constrain the ionization mechanism of the ISM, i.e., distinguish whether the observed emission originates from AGN feedback or star formation (e.g., Merluzzi et al. 2013). In partic-

ular, simultaneous observations of Hα and Hβ emission lines enable the derivation of dust extinction maps that can be studied along with Hα-derived SFR maps to study the star formation activity of galaxies on local scales (Nelson et al. 2016; Jafariyazani et al. 2019).

Bibliography

Abazajian, K., Adelman-McCarthy, J. K., Agüeros, M. A., et al. 2004, The Second Data Release of the Sloan Digital Sky Survey, AJ, 128, 502

Abazajian, K. N., Adelman-McCarthy, J. K., Agüeros, M. A., et al. 2009, The Seventh Data Release of the Sloan Digital Sky Survey, ApJS, 182, 543

Arnouts, S., Cristiani, S., Moscardini, L., et al. 1999, Measuring and modelling the redshift evolution of clustering: the Hubble Deep Field North, MNRAS, 310, 540

Balogh, M. L., Navarro, J. F., & Morris, S. L. 2000, The Origin of Star Formation Gradients in Rich Galaxy Clusters, ApJ, 540, 113

Bekki, K., Couch, W. J., & Shioya, Y. 2002, Passive Spiral Formation from Halo Gas Starvation: Gradual Transformation into S0s, ApJ, 577, 651

Bekki, K. 2014, Galactic star formation enhanced and quenched by ram pressure in groups and clusters, MNRAS, 438, 444

Bernardi, M., Shankar, F., Hyde, J. B., et al. 2010, Galaxy luminosities, stellar masses, sizes, velocity dispersions as a function of morphological type, MNRAS, 404, 2087

Bertin, E., & Arnouts, S. 1996, SExtractor: Software for source extraction., A&AS, 117, 393

Blanton, M. R., Hogg, D. W., Bahcall, N. A., et al. 2003, The Broadband Optical Properties of Galaxies with Redshifts 0.02<z<0.22, ApJ, 594, 186

Böhringer, H., Briel, U. G., Schwarz, R. A., et al. 1994, The structure of the Virgo cluster of galaxies from Rosat X-ray images, Nature, 368, 828

Boissier, S., Boselli, A., Duc, P.-A., et al. 2012, The GALEX Ultraviolet Virgo Cluster Survey (GUViCS). II. Constraints on star formation in ram-pressure stripped gas, A&A, 545, A142

Boselli, A., Fossati, M., Cuillandre, J. C., et al. 2018, A Virgo Environmental Survey Tracing Ionised Gas Emission (VESTIGE). III. Star formation in the stripped gas of NGC 4254, A&A, 615, A114

Bothun, G. D., & Dressler, A. 1986, Blue Disk Galaxies in the Coma Cluster: Analongs to Z = 0.5 Cluster Members?, ApJ, 301, 57

Brinchmann, J., Charlot, S., White, S. D. M., et al. 2004, The physical properties of star-forming galaxies in the low-redshift Universe, MNRAS, 351, 1151

Bruzual, G. & Charlot, S. 2003, Stellar population synthesis at the resolution of 2003, MNRAS, 344, 1000

Calzetti, D., Armus, L., Bohlin, R. C., et al. 2000, The Dust Content and Opacity of Actively Star-forming Galaxies, ApJ, 533, 682

Chabrier, G. 2003, Galactic Stellar and Substellar Initial Mass Function, PASP, 115, 763

Chary, R. & Elbaz, D. 2001, Interpreting the Cosmic Infrared Background: Constraints on the Evolution of the Dust-enshrouded Star Formation Rate, ApJ, 556, 562

Chung, A., van Gorkom, J. H., Kenney, J. D. P., et al. 2007, Virgo Galaxies with Long One-sided HI Tails, ApJL, 659, L115

Chung, A., van Gorkom, J. H., Kenney, J. D. P., et al. 2009, VLA Imaging of Virgo Spirals in Atomic Gas (VIVA). I. The Atlas and the H I Properties, AJ, 138, 1741

Conroy, C. 2013, Modeling the Panchromatic Spectral Energy Distributions of Galaxies, ARAA, 51, 393

Cortese, L., Marcillac, D., Richard, J., et al. 2007, The strong transformation of spiral galaxies infalling into massive clusters at z $\sim$ 0.2, MNRAS, 376, 157

Cowie, L. L. & Songaila, A. 1977, Thermal evaporation of gas within galaxies by a hot intergalactic medium, Nature, 266, 501

Crowl, H. H. & Kenney, J. D. P. 2008, The Stellar Populations of Stripped Spiral Galaxies in the Virgo Cluster, AJ, 136, 1623

Elbaz, D., Daddi, E., Le Borgne, D., et al. 2007, The reversal of the star formation-density relation in the distant universe, A&A, 468, 33

Elbaz, D., Dickinson, M., Hwang, H. S., et al. 2011, GOODS-Herschel: an infrared main sequence for star-forming galaxies, A&A, 533, A119

Ferrarese, L., Côté, P., Cuillandre, J.-C., et al. 2012, The Next Generation Virgo Cluster Survey (NGVS). I. Introduction to the Survey, ApJS, 200, 4

Fujita, Y. & Nagashima, M. 1999, Effects of Ram Pressure from the Intracluster Medium on the Star Formation Rate of Disk Galaxies in Clusters of Galaxies, ApJ, 516, 619

Fujita, Y. 2004, Pre-Processing of Galaxies before Entering a Cluster, PASJ, 56, 29

Gill, S. P. D., Knebe, A., & Gibson, B. K. 2005, The evolution of substructure - III. The outskirts of clusters, MNRAS, 356, 1327

Giovanelli, R., Haynes, M. P., Kent, B. R., et al. 2005, The Arecibo Legacy Fast ALFA Survey. I. Science Goals, Survey Design, and Strategy, AJ, 130, 2598

Gunn, J. E., & Gott, J. R. 1972, On the Infall of Matter Into Clusters of Galaxies and Some Effects on Their Evolution, ApJ, 176, 1

Haynes, M. P., Giovanelli, R., Martin, A. M., et al. 2011, The Arecibo Legacy Fast ALFA Survey: The α.40 H I Source Catalog, Its Characteristics and Their Impact on the Derivation of the H I Mass Function, AJ, 142, 170

Haynes, M. P., & Giovanelli, R. 1984, Neutral hydrogen in isolated galaxies. IV. Results for the Arecibo sample., AJ, 89, 758

Haynes, M. P., Giovanelli, R., Kent, B. R., et al. 2018, The Arecibo Legacy Fast ALFA Survey: The ALFALFA Extragalactic H I Source Catalog, ApJ, 861, 49

Hester, J. A., Seibert, M., Neill, J. D., et al. 2010, IC 3418: Star Formation in a Turbulent Wake, ApJL, 716, L14

Hwang, H. S., Park, C., Elbaz, D., et al. 2012, Activity in galactic nuclei of cluster and field galaxies in the local universe, A&A, 538, A15

Hwang, H. S., Geller, M. J., Diaferio, A., et al. 2012, A WISE View of a nearby Supercluster A2199, ApJ, 752, 64

Hwang, H. S., Geller, M. J., Kurtz, M. J., et al. 2012, SHELS: Optical Spectral Properties of WISE 22μm Selected Galaxies, ApJ, 758, 25

Ilbert, O., Arnouts, S., McCracken, H. J., et al. 2006, Accurate photometric redshifts for the CFHT legacy survey calibrated using the VIMOS VLT deep survey, A&A, 457, 841

Jafariyazani, M., Mobasher, B., Hemmati, S., et al. 2019, Spatially Resolved Properties of Galaxies from CANDELS+MUSE: Radial Extinction Profile and Insights on Quenching, ApJ, 887, 204

Jaffé, Y. L., Smith, R., Candlish, G. N., et al. 2015, BUDHIES II: a phase-space view of H I gas stripping and star formation quenching in cluster galaxies, MNRAS, 448, 1715

Jarrett, T. H., Cohen, M., Masci, F., et al. 2011, The Spitzer-WISE Survey of the Ecliptic Poles, ApJ, 735, 112

Kapferer, W., Sluka, C., Schindler, S., et al. 2009, The effect of ram pressure on the star formation, mass distribution and morphology of galaxies, A&A, 499, 87

Kauffmann, G., Heckman, T. M., White, S. D. M., et al. 2003, Stellar masses and star formation histories for 105 galaxies from the Sloan Digital Sky Survey, MNRAS, 341, 33

Kennicutt, R. C. 1998, The Global Schmidt Law in Star-forming Galaxies, ApJ, 498, 541

Kennicutt, R. C., & Evans, N. J. 2012, Star Formation in the Milky Way and Nearby Galaxies, ARAA, 50, 531

Kenney, J. D. P., Geha, M., Jáchym, P., et al. 2014, Transformation of a Virgo Cluster Dwarf Irregular Galaxy by Ram Pressure Stripping: IC 3418 and Its Fireballs, ApJ, 780, 119

Kim, S., Rey, S.-C., Jerjen, H., et al. 2014, The Extended Virgo Cluster Catalog, ApJS, 215, 22

Kim, S., Rey, S.-C., Bureau, M., et al. 2016, Large-scale Filamentary Structures around the Virgo Cluster Revisited, ApJ, 833, 207

Ko, J., Hwang, H. S., Lee, J. C., et al. 2013, The Mid-infrared and Near-ultraviolet Excess Emissions of Quiescent Galaxies on the Red Sequence, ApJ, 767, 90

Koopmann, R. A., & Kenney, J. D. P. 2004, Massive Star Formation Rates and Radial Distributions from Hα Imaging of 84 Virgo Cluster and Isolated Spiral Galaxies, ApJ, 613, 851

Koopmann, R. A., & Kenney, J. D. P. 2004, Hα Morphologies and Environmental Effects in Virgo Cluster Spiral Galaxies, ApJ, 613, 866

Kronberger, T., Kapferer, W., Ferrari, C., et al. 2008, On the influence of ram-pressure stripping on the star formation of simulated spiral galaxies, A&A, 481, 337

Kroupa, P. 2001, On the variation of the initial mass function, MNRAS, 322, 231

Larson, R. B., Tinsley, B. M., & Caldwell, C. N. 1980, The evolution of disk galaxies and the origin of S0 galaxies, ApJ, 237, 692

Lee, B., Chung, A., Tonnesen, S., et al. 2017, The effect of ram pressure on the molecular gas of galaxies: three case studies in the Virgo cluster, MNRAS, 466, 1382

Lee, J. C., Hwang, H. S., & Ko, J. 2013, The Calibration of Star Formation Rate Indicators for WISE 22 μm-Selected Galaxies in the Sloan Digital Sky Survey, ApJ, 774, 62

Mamon, G. A., Sanchis, T., Salvador-Solé, E., et al. 2004, The origin of HI-deficiency in galaxies on the outskirts of the Virgo cluster. I. How far can galaxies bounce out of clusters?, A&A, 414, 445

Martig, M., Bournaud, F., Teyssier, R., et al. 2009, Morphological Quenching of Star Formation: Making Early-Type Galaxies Red, ApJ, 707, 250

Mateos, S., Alonso-Herrero, A., Carrera, F. J., et al. 2012, Using the Bright Ultrahard XMM-Newton survey to define an IR selection of luminous AGN based on WISE colours, MNRAS, 426, 3271

McGee, S. L., Balogh, M. L., Bower, R. G., et al. 2009, The accretion of galaxies into groups and clusters, MNRAS, 400, 937

McLaughlin, D. E. 1999, Evidence in Virgo for the Universal Dark Matter Halo, ApJL, 512, L9

Mei, S., Blakeslee, J. P., Côté, P., et al. 2007, The ACS Virgo Cluster Survey. XIII. SBF Distance Catalog and the Three-dimensional Structure of the Virgo Cluster, ApJ, 655, 144

Merluzzi, P., Busarello, G., Dopita, M. A., et al. 2013, ACCESS - V. Dissecting ram-pressure stripping through integral-field spectroscopy and multiband imaging, MNRAS, 429, 1747

Moore, B., Katz, N., Lake, G., et al. 1996, Galaxy harassment and the evolution of clusters of galaxies, Nature, 379, 613

Nelson, E. J., van Dokkum, P. G., Momcheva, I. G., et al. 2016, Spatially Resolved Dust Maps from Balmer Decrements in Galaxies at z $\sim$ 1.4, ApJL, 817, L9

Oman, K. A., Hudson, M. J., & Behroozi, P. S. 2013, Disentangling satellite galaxy populations using orbit tracking in simulations, MNRAS, 431, 2307

Oman, K. A. & Hudson, M. J. 2016, Satellite quenching time-scales in clusters from projected phase space measurements matched to simulated orbits, MNRAS, 463, 3083

Park, C., & Hwang, H. S. 2009, Interactions of Galaxies in the Galaxy Cluster Environment, ApJ, 699, 1595

Poggianti, B. M., Moretti, A., Gullieuszik, M., et al. 2017, GASP. I. Gas Stripping Phenomena in Galaxies with MUSE, ApJ, 844, 48

Ramatsoku, M., Serra, P., Poggianti, B. M., et al. 2019, GASP - XVII. H I imaging of the jellyfish galaxy JO206: gas stripping and enhanced star formation, MNRAS, 487, 4580

Rhee, J., Smith, R., Choi, H., et al. 2017, Phase-space Analysis in the Group and Cluster Environment: Time Since Infall and Tidal Mass Loss, ApJ, 843, 128

Roediger, E. 2009, Ram pressure stripping of disk galaxies in galaxy clusters, Astronomische Nachrichten, 330, 888

Salpeter, E. E. 1955, The Luminosity Function and Stellar Evolution., ApJ, 121, 161

Smith, R. J., Lucey, J. R., Hammer, D., et al. 2010, Ultraviolet tails and trails in cluster galaxies: a sample of candidate gaseous stripping events in Coma, MNRAS, 408, 1417

Steinhauser, D., Schindler, S., & Springel, V. 2016, Simulations of ram-pressure stripping in galaxy-cluster interactions, A&A, 591, A51

Strateva, I., Ivezić, Ž., Knapp, G. R., et al. 2001, Color Separation of Galaxy Types in the Sloan Digital Sky Survey Imaging Data, AJ, 122, 1861

Vollmer, B. 2009, A holistic view on ram pressure stripping in the Virgo cluster. The first complete model-based time sequence, A&A, 502, 427

von der Linden, A., Wild, V., Kauffmann, G., et al. 2010, Star formation and AGN activity in SDSS cluster galaxies, MNRAS, 404, 1231

Vulcani, B., Poggianti, B. M., Gullieuszik, M., et al. 2018, Enhanced Star Formation in Both Disks and Ram-pressure-stripped Tails of GASP Jellyfish Galaxies, ApJL, 866, L25

West, A. A., Garcia-Appadoo, D. A., Dalcanton, J. J., et al. 2010, H I-Selected Galaxies in the Sloan Digital Sky Survey. I. Optical Data, AJ, 139, 315

Wright, E. L., Eisenhardt, P. R. M., Mainzer, A. K., et al. 2010, The Wide-field Infrared Survey Explorer (WISE): Mission Description and Initial On-orbit Performance, AJ, 140, 1868

Yoon, H., Chung, A., Smith, R., et al. 2017, A History of HI Stripping in Virgo: A Phase-space View of VIVA Galaxies, ApJ, 838, 81

요 약

처녀자리 (Virgo) 은하단에서 충차압에 의한 가스 손실 (ram pressure stripping) 을 겪는 은하들의 항성 형성 활동 (star formation activity) 이 시간에 따라 어떻게 변하는지에 대한 연구를 수행하였다. 먼저, VLA Imaging survey of Virgo galaxies in Atomic gas (VIVA)를 통해서 고해상도 중성 수소 (HI) 선 관측이 이루어진 48개의 은하들을 기반으로 연구를 시작하였다. 이 48개의 은하들은 중성 수소 형태 (HI morphology), 중성 수소 결핍 (HI deficiency), 그리고 중성 수소 대 항성 원반 범위의 비율 (relative extent to the stellar disk) 으로 각각 다른 가스 손실 단계로 분류가 가능하였다. 그 후, 중성 수소 대 항성 질량비 (HI mass fraction)와 투영 위상 공간 (projected phase space) 에서의 위치를 결합하여 새로운 은하 분류 방법을 적용하며 최종 샘플 수가 241개로 늘어났다. 다른 가스 손실 단계에서의 항성 형성 활동의 차이를 비교하기 위해 다양한 항성 형성 추적자 (star formation tracers) 을 사용하는데, $g - r$, *WISE* [3.4] − [12] 색지수, 그리고 항성 질량과 항성 형성률로 정의 된 starburstiness이라는 매개 변수를 사용했다. 가스 손실을 활발하게 겪고 있는 은하들의 적분 된 항성 형성 활동이 향상이 됐다는 명확한 증거는 찾을 수가 없었다. 반면에 충차압의 강도가 증가하면서 전체적으로 항성 형성이 억제되는 현상을 확인할 수 있었고, 이 점은 선행 연구의 결과와 일치하였다. 충차압에 의해 가스 손실이 일어나면서 항성 형성 향상이 있다한들, 기껏해야 국지적으로 미미하거나 그러한 은하들이 총 샘플에서 작은 부분을 차지하는 것으로 보인다. 본 연구에서 강조하고 싶은 점은, 중성 수소 대 항성 질량비와 투영 위상 공간에서의 위치를 결합을 하여 은하를 분류할 경우, 각각 다른 손실 단계에 있는 은하들을 추적할 수 있을 뿐더러, 이 방법은 고해상도 중성 수소 자료가 없는 은하단에도 적용이 가능할 것으로 보인다.

주요어: 은하: 은하단: 일반 − 은하: 은하단: Virgo − 은하: 진화 − 은하: 항성 형성

학 번: 2018-26181

감 사 의 글

감사의 글을 쓰려고 하다보니, 지난 2년간 서울대에서 공부를 하면서 다양한 사람들을 만나 너무나 많은 값진 추억들을 쌓았다는 것을 다시 한번 깨닫게 되네요. 감사의 글에서 제가 느끼고 배운 모든 점을 담아내진 못하겠지만, 나름 신중하게 적어봅니다.

먼저, 좋은 환경 속에서 연구를 할 수 있게 해주신 저의 지도교수님, 이명균 교수님께 감사의 말씀을 드립니다. 신입생 시절 교수님의 관측법 수업을 들으면서 어버버거리던때가 엊그제 같은데, 항상 인자하신 미소를 지으시면서 피드백을 주시고, 제가 부족한 점이 있어도 이해해주셔서 제가 지난 2년간 많은 성장을 할 수 있었던게 아닌가 싶습니다. 특히나 어떤 상황에서도 긍정적이여야한다는 점을 강조해주시고, 항상 학생의 행복에 관심을 기울어주시는 교수님 덕분에 저도 교수님을 닮아 긍정적으로 변해간 것 같습니다. 천문학 뿐만에서도 아니라 인생에서도 좋은 선생님이 되어주셨었던 점 진심으로 감사드리며, 교수님께서 항상 행복하시길 바라겠습니다.

다음으로는 이 학위 논문의 연구에 큰 기여 및 지도를 해주신 황호성 박사님께 감사 인사를 올립니다. 박사님과 첫 면담 때 잔뜩 긴장한 상태로 고등과학원에 갔었는데, 활짝 웃으시면서 커피부터 마시자며 머그컵을 주셨던 모습이 아직도 생생합니다. 그 때만해도 실수를 하거나 뭔가를 모르면 스스로 자책을 많이 하던 시절이였는데, 쫄지 말라고 하시면서 제 질문에 항상 친절하게 대답해주셔서 제가 자신감을 많이 되찾을 수 있었습니다. 바쁘실텐데에도 불구하고 시간을 내셔서 스카이프로 제 연구를 봐주시고, 늦은 시간에도 제 이메일에 성심성의껏 답변해주셔서 너무나 감사합니다. 그 외에도, 연구가 잘 되질 않아 박사님께 하소연을 했던 적이 한두번이 아니였는데, 그 때마다 긍정적으로 말씀해주시고 위로해주셨던 덕분에 이 연구를 무사히 잘 마칠 수 있었습니다.

이 연구를 수행할 수 있게 큰 도움을 주신 정애리 교수님과 혜인 언니에게 감사하다고 말씀을 드리고 싶습니다. Virgo cluster와 ram pressure stripping 전문가이신 두분을 모셔서 함께 연구를 할 수 있어서 정말 든든했습니다. 혜인 언니는 곧 호주에서 뵙기를...!

그리고 저널 논문의 내용을 개선하는데 도움을 주신 이종철 박사님께도 감사 인사를 드립니다. 다음으로 논문 심사를 맡아주신 구본철 교수님과 임명신 교수님께도 감사의 말씀을 전해드립니다. 대학원에서 구본철 교수님의 강의를 들을 수 있었다는 점에 너무 감사하고, 제게 천문학의 기초 지식을 쌓는데 큰 도움이 되었습니다. 대학원을 다니면서 임명신 교수님의 강의를 들어보지 못한게 많은 아쉬움으로 남습니다.

다음으로는 Obs Cos 팀원들께 감사 인사를 전합니다. 학회 다녀올 때나 팀 관련 일이 생길 때 나서서 담담하게 리드하는 지수 언니 덕분에 매우 든든했습니다. 팀에서 워크샵 계획을 담당하는 Brian 덕분에 교수님, 그리고 팀원들과 함께 더 많은 추억을 쌓을 수 있었다는 점에 대해 감사하다고 전해드리고 싶습니다. 이번에는 코로나 때문에 워크샵을 가지 못해서 아쉽네요. 그리고 제가 대학원 새내기 시절부터 관측법 관련 질문을 많이 받은 정환오빠, 항상 친절하게 설명해줘서 너무 감사합니다. 팀에서 ram pressure stripping 연구하는 팀원이 또 있어서 반가웠고 앞으로의 우주 해파리 은하 연구 결과를 기대하겠습니다. 지금은 석사 전문연으로 취직해서 열심히 일하고 있을 강일이, 신입생 때부터 수업 같이 들으면서 챙겨줬던 점 항상 고맙게 생각하고 있어. 항상 생각이 깊고 다른 사람 배려를 먼저 하는 성아, 건강히 잘 지내며 즐겁게 연구에 임할 수 있기를 바래! 마지막으로, 팀미팅 때마다 새로운 그림들을 가져오면서 무서운 속도로 연구하는 유정이. 같이 수업 들을 때도 그랬지만, 뭐든 빠르게 습득하고 자기만의 지식과 스킬로 삼는 유정이 보고 배울게 많다고 느꼈어. 이번에는 특히 학위 proposal와 defense 준비하면서 모든 팀원들로부터 많은 도움을 받았었는데, 팀원들 없었으면 어쩔 뻔...도움을 요청하면 본인 일인 마냥 나서서 도와주는 팀원들이 있었기에 대학원 생활도 순탄하게 흘러갔던 것 같습니다.

팀사람들 외에도, 대학원 생활하면서 제게 큰 힘이 되어주고 웃게 해준 학과 친구들에게 고맙다고 전하고 싶습니다. 외국에서의 오랜 생활 때문에 한국에서는 친구가 없었는데, 서울대에서 소중한 인연들이 많이 만들고 간다는 점에 매우 감사하게 느낍니다. 시크하면서도 개그욕심 많고 항상 침착하게 일 잘하는 승학이, 무슨 일이 닥쳐도 긍정적이고 사람을 편하게 만들어주는 주연이. 신입생 시절에 대학원 생활에 적응하면서 꽤나 힘들어했지만 둘 덕분에 많이 든든했어. 주연이는 특히 1년간 연구실을 같이 쓰면서 쌓게 된 추억들이

너무 많고 덕분에 웃음이 끊기질 않았었던 점, 너무 감사해. 다음으로는 내 동갑내기 친구들, 가인이와 수현이. 나랑 개그코드와 의식적 흐름도 잘 맞는 가인이, 덕분에 배 근육이 아프도록 많이 웃고 다녔던 것 같다. 항상 사람들과 얘기할 때 활짝 웃어주고 뭐든 신나하는 행복바이러스 수현이, 항상 행복하길! 입학했을 때 같은 문씨 선배가 있어서 처음부터 반가웠던 상혁 오빠, 요즘은 손등을 잘 찍고 다니는 것 같아서 뿌듯합니다. 코드만 보면 뭐가 문제인지 바로 알아차리는 호진 오빠, 덕분에 여러 번 도움을 많이 받았습니다. 똑똑하고 코딩도 잘하는 윤수, 이번에 같이 연구실 쓰면서 좀 더 친해진 것 같아 기쁩니다. 가끔씩 휴게실에서 마주칠 때마다 같이 잡담을 나눈 무건 오빠, 최근이 되어서야 같이 밥 먹으며 서로를 좀 더 알게 된 하림이, 자주 뵙지 못했지만 뵐 때 마다 친절하신 소피아 언니, 항상 응원합니다. 그리고 지금은 졸업하셔서 학교에 더 이상 안 계시지만 잠깐이나마 알고 지냈던 윤영 언니, 재진 선배, 그리고 하은 선배. 윤영 언니는 세상이 좁다면 정말 좁다고 할 수 있을 정도로 우연찮게 UCLA에서 만나게 되어서 서울대에서까지 인연을 이어가게 되어 정말 반가웠습니다. 처음 뵀을 때부터 저를 잘 챙겨주시고 편하게 대해주셨던 재진 선배, 특히 신입생 시절 큰 힘이 되어주어 감사하다고 전해드리고 싶습니다. 고등과학원 다니던 시절, 여러 박사님들과 교수님들 사이에서 혼자 뻘쭘해할때 말 걸어주시고 서로 티격태격할 정도로 친해졌던 하은 선배께도 감사의 말씀 전해드립니다. 그 외에도, 대학원 생활을 하면서 제게 친절히 대해주셨던 서울대에 계신 분들 뿐만 아니라 모든 천문학과 사람들께 감사인사를 드립니다.

그리고 마지막으로, 항상 저를 응원해주시는 제 부모님께 감사의 인사를 올립니다. 좋아하는 공부를 하면서 행복하게 살기를 바란다고 말씀해주시고, 저를 믿어주시고 사랑해주셔서 제가 여기까지 올 수 있었고, 앞으로도 살아가면서 제 꿈을 이루는데 큰 힘이 될 것입니다. 항상 엄마 아빠가 자랑스럽게 생각할 수 있는 딸이 되도록 노력할게. 오래오래 건강하셔서 제 성장과정을 계속 지켜봐주시면 감사하겠습니다. 많이 사랑합니다!!

2020년 7월

문재연 올림